矿物岩石地球化学通报
Bulletin of Mineralogy, Petrology and Geochemistry
Vol.43, 2024

地核物质成分、结构与形核研究进展

高宸[1],Kai-Ming Ho[2],孙阳[1*]

1. 厦门大学 物理科学与技术学院, 厦门 361005; 2. 爱荷华州立大学 物理与天文系, 美国 埃姆斯市 50011

摘　要：地核由液态外核和固态内核组成,其主要化学成分是铁,此外还包含少量镍和轻质元素,这些元素在内、外核中的含量存在较大争议。地震波数据显示,内地核具有显著的各向异性,可能与其晶体结构和物态密切相关,但研究者们对此尚未完全理解。同时,内核的年龄及结晶过程也存在许多谜团。地核成分、结构及其形成过程对于理解地球深部演变至关重要。近年来,随着高压实验和第一性原理计算模拟的发展,各种物理和化学手段被广泛应用于研究地核物质物性问题。本文总结了近十年来地核物质成分、结构及结晶过程的研究进展,概述了镍与轻元素在内、外核中的含量及其对地核结构、密度和地震波速等性质影响的研究结果,指出了探究地核多元物质固液相图的重要性。此外,本文还简要总结了与内核年龄相关的研究工作,阐释了在探究地核演化过程中发现的理论难题与悖论。本文可为未来的地核研究提供一定的参考。

关　键　词：地球地核;地核组分;内地核结构;内地核形核

中图分类号：P591^{+}.2　　**doi:** 10.3724/j.issn.1007-2802.20240094

Progress in the study of the composition, structure and nucleation of the Earth′s core

GAO Chen[1], HO Kai-Ming[2], SUN Yang[1*]

1. *College of Physical Science and Technology, Xiamen University, Xiamen* 361005, *China;*
2. *Department of Physics and Astronomy, Iowa State University, Ames IA,* 50011, *USA*

Abstract: The Earth′s core located at the center of the Earth consists of a liquid outer core and a solid inner core. Its main chemical component is iron, with small amounts of nickel and light elements. Contents of those elements in the inner and outer cores are of considerably debated. Seismic data show that the inner core has significant anisotropy, which could be closely related to the crystal structure and physical state of its components, though this relationship is not yet fully understood by researchers. Meanwhile, the age and crystallization process of the inner core remain enigmatic. The composition, structure, and formation processes of the Earth's core are crucial for understanding the evolution of the Earth′s interior parts. In recent years, with the advancement of high-pressure experiments and first-principles computational simulations, various physical and chemical methods have been extensively applied to the study of physical properties of materials in the Earth's core. In this paper, we have summarized progresses of researches over the past decade on the composition, structure, and crystallization processes of the Earth′s core, briefly reviewed studies on contents of nickel and light elements in the inner and outer cores and their influences on properties such as the structure, density, and seismic wave velocity of the Earth's core, and emphasized the importance for developing solid-liquid phase diagrams for multi-component materials of the Earth's core. In addition we have also briefly summarized progresses of researches related to the age of the inner core, and elucidated the theoretical challenges and paradoxes encountered in researches for exploring the evolution of the Earth's core. Our paper aims to provide a reference for future studies of the Earth′s core.

Key words: Earth′s core; chemical composition of the Earth's core; structure of the inner core; nucleation of the inner core

收稿编号:2024-0099,2024-05-31 收到,2024-07-09 改回
基金项目:国家自然科学基金资助项目(42374108)
第一作者简介:高宸(2001—),男,博士研究生,研究方向:地核物质相变. E-mail:chgao@stu.xmu.edu.cn.
*通信作者简介:孙阳(1990—)男,副教授,研究方向:极端条件下物性与相变. E-mail:yangsun@xmu.edu.cn.

引用此文:
高宸,Kai-Ming Ho,孙阳. 2024. 地核物质成分、结构与形核研究进展. 矿物岩石地球化学通报,doi: 10.3724/j.issn.1007-2802.20240094
Gao C,Ho K,Sun Y. 2024. Progress in the study of the composition, structure and nucleation of the Earth′s core. Bulletin of Mineralogy, Petrology and Geochemistry,doi: 10.3724/j.issn.1007-2802.20240094

0 引言

约46亿年前，太阳系中的尘埃与气体聚集成微行星，并在引力与碰撞的作用下逐步演化成原始地球。早期地球的表面覆盖着熔融硅酸盐组成的岩浆洋。微行星等物体撞击地球后，其内部的金属会解体成液滴，并缓慢沉降到岩浆洋底部。在此过程中，金属液滴与硅酸盐溶体中的元素重新达到化学平衡。金属液滴在原始地幔表面沉积，形成金属层。金属层在达到一定厚度后会解体并快速穿过原始地幔，最终聚集在地球中心，形成富铁的熔融地核。当地球生长到一定规模时，环境的氧化性增强，最终导致核幔分异停止(Wade and Wood，2005；Wood et al.，2006；Halliday and Wood，2009；Hirose et al.，2021)。熔融地核不断冷却散热，当其温度降至某一临界值时，液态地核开始结晶，从而形成固态内核。

地核的半径约为3480 km，超过地球半径(约6371 km)的一半，其中内核的半径约为1221 km。地核体积约为地球体积的六分之一，而其质量则占到地球的三分之一(Li and Fei，2014)。地核内部压强随深度变化显著。在核幔边界(core-mantle boundary，CMB)处，压强约为136 GPa，在内核边界(inner core boundary，ICB)处，压强约为329 GPa，而在地核中心压强则高达364 GPa。受地核物质熔点与热力学性质的影响，地核的温度存在较大不确定性。根据当前的研究，CMB的温度为3000~5000 K(Stixrude et al.，2009；Fiquet et al.，2010；Nimmo，2015；Hirose et al.，2021)，ICB的温度为5000~7000 K(Alfè et al.，2007；Anzellini et al.，2013；Li and Fei，2014；Belonoshko et al.，2021)。图1a展示了地球的简易剖面图，反映了各项参数随半径的变化。

Dziewonski和Anderson(1981)提出Preliminary Reference Earth Model (PREM)来描述地球内部的物理和化学性质，反映地球密度与地震波速随深度的变化。如图1b所示，PREM是研究地核组成与结构等问题的重要标准。铁(Fe)是地核的主要元素，然而

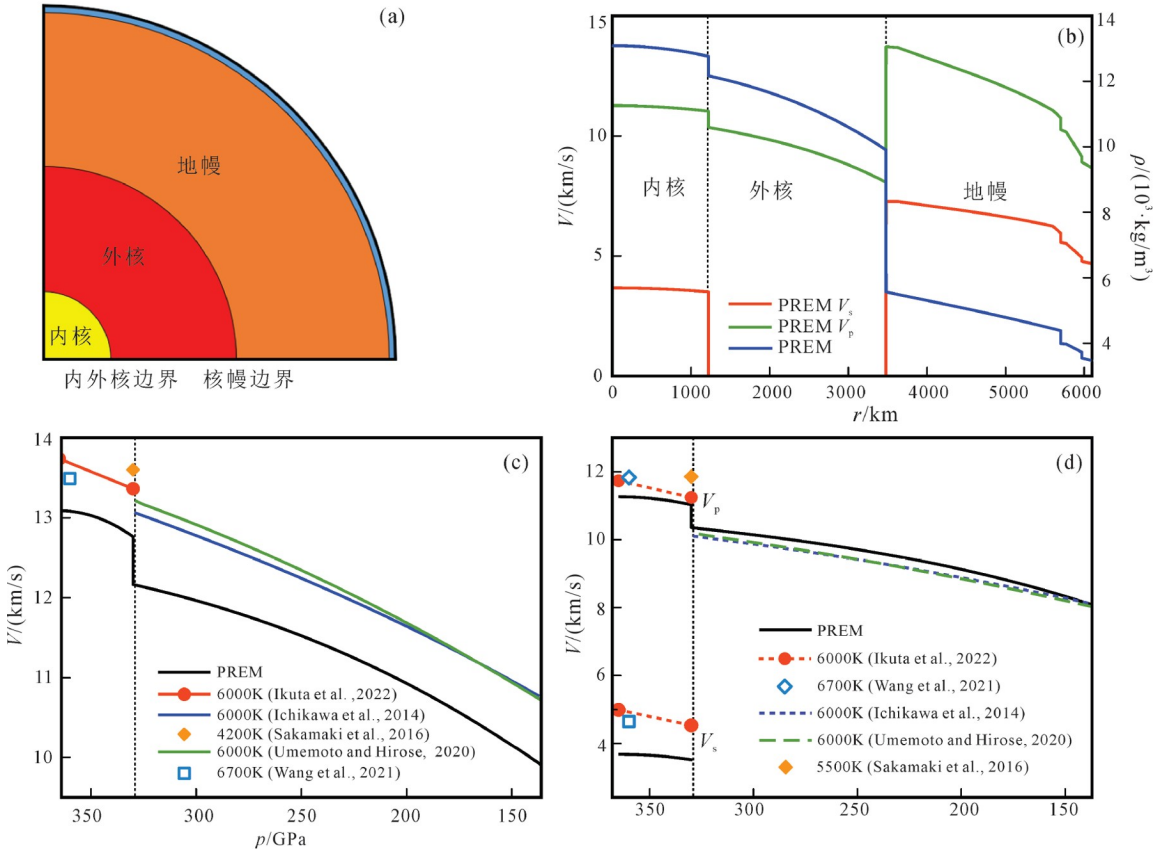

V_s—剪切波速；V_p—压缩波速

图1 (a)地球简易剖面图；(b)PREM的地震波波速、密度随半径的变化(修改自Dziewonski and Anderson，1981)；(c)Fe的密度随压强的变化关系；(d)Fe的波速与压强的关系

Fig.1 (a) Schematic diagram of the Earth，with the pressure，temperature and mass as a function of radius；(b) The seismic wave velocity and density as a function of radius in the PREM(modified from Dziewonski and Anderson，1981)；(c) The density of Fe as a function of pressure；(d) The sound velocity of Fe as a function of pressure

PREM显示,内、外核的密度ρ比纯铁低,外核的压缩波速V_p比纯铁快,而内核的压缩波速V_p和剪切波速V_s较纯铁低(Dziewonski and Anderson,1981;Poirier,1994;Anderson and Ahrens,1994;Ichikawa et al.,2014;Sakamaki et al.,2016;Ikuta et al.,2022)(图1c、1d)。因此,研究者们认为地核中存在其他轻质元素。本文整理了近十年来碳(C)、氢(H)、氧(O)、硫(S)、硅(Si)和镍(Ni)等地核潜在元素的研究成果,介绍了这些元素在地核中的配分及其对地核的热力学性质和弹性性质的影响;简述了内核波速的各向异性及其可能的产生原因;介绍了研究者们对内核中铁晶体结构的争论以及超离子物态对地核性质的影响;最后,简单介绍了地球发电机模型,并讨论了有关内核形成的问题与悖论。

1　地核组分

1.1　地核组分的研究方法

地核的主要成分是Fe,另包含5%~15%的Ni(质量分数,下同)和约10%左右的轻质元素(Birch,1952;Dziewonski and Anderson,1981;McDonough and Sun,1995;Alfè et al.,2007)。这些轻质元素对地核的热力学和动力学性质以及地磁场的产生和维持等均有重要影响。由于缺乏地核物质样本,研究者们常通过高温高压实验和理论计算模拟,探究这些元素在地核条件下的性质,以此推断其在地核中的含量。实验上通常用金刚石对顶砧(Diamond Anvil Cell,DAC)、大压机或冲击波模拟高压环境,并运用激光或电阻加热模拟高温环境。理论计算上通常使用密度泛函理论(Density Functional Theory,DFT)和分子动力学模拟(Molecular Dynamics simulation,MD)来研究地核物质在高温高压下的物性。基于这些实验和理论方法,可以利用以下手段约束地核中轻元素的组分:

(1)地球演化约束。地球在早期增生时期获得了大量元素。在核幔分异过程中,硅酸盐溶体与金属熔体液滴达到化学平衡,部分亲铁元素会转移到金属熔体液滴中,并随其一同沉入地核(Wade and Wood,2005;Wood et al.,2006;Hirose et al.,2021)。可以通过模拟核幔分异条件下物质的热化学平衡过程,探究轻质元素在金属熔体和硅酸盐熔体中的配分系数($D^{Fe/Si}$),再结合地球在早期增生过程中获得的元素总量,为确定地核组分提供约束(Yuan and Steinle-Neumann,2020)。此外,核幔分异会改变硅酸盐熔体中部分元素的同位素组成,这一特性也为确定地核组分提供帮助(Fitoussi et al.,2009)。有些元素可能在晚期增生时期来到地球,未经历核幔分异过程,则需要进一步分析它们的含量(Wang et al.,2024)。

(2)地震波数据约束。地震波数据为地核组分提供了关键约束,真实的地核组分应同时反映内外地核的密度、波速及泊松比等地震观测性质(Antonangeli et al.,2010;Yokoo et al.,2019;Ichikawa and Tsuchiya,2020)。

(3)热力学与化学平衡约束。在地核条件下,大部分轻质元素可与铁形成共晶系统,熔融的外核要能够结晶出富铁的内核,其组分必须落在铁的液相区域。因此,地核条件下铁与轻质元素合金的固液热力学相图对约束轻质元素的含量十分重要(Ozawa et al.,2010;Li and Fei,2014;Morard et al.,2017)。通过固液共存模拟,可确定轻质元素在内外核中的配分系数,从而计算ICB处的固液化学成分(Li et al.,2019;Yuan and Steinle-Neumann,2023)。

1.2　地核组分研究

1.2.1　氢元素　H是宇宙中含量最为丰富的元素,地球能够从宇宙中获取大量的H(McDonough and Sun,1995)。低温低压下H表现出亲硅性,Clesi等(2018)和Malavergne等(2019)在20 GPa下测得H在金属和硅酸盐中的配分系数较低(约为0.2)。也有一些实验(Okuchi,1997;Iizuka-Oku et al.,2017;Tagawa et al.,2021;Oka et al.,2022)和理论(Li Y G et al.,2020;Yuan and Steinle-Neumann,2023)研究表明,H在高压下(大于20~30 GPa)具有亲铁性(图2a)。H的金属-硅酸盐配分系数和内外核配分系数约为5~50和0.5~0.8(Li Y G et al.,2020;Oka et al.,2022;Hikosaka et al.,2022;Yuan and Steinle-Neumann,2023)。Li Y G等(2020)认为,如果地球上的水来自早期增生阶段,由于较高的配分系数,76%的H会随金属液滴进入地核,使地核成为一个“大水库”;反之,如果地球上的水主要来自后薄层增生,则地核几乎不含水。Tagawa等(2021)利用多种模型估算出地球在增生过程中获得的H含量,结合H的金属-硅酸盐配分系数,提出地核的H含量为0.3%~0.6%。Yuan和Steinle-Neumann(2023)计算了H的内外核配分系数,认为在地核H含量为0.3%的假设下,内外核中H的质量可能是海洋的1倍和33倍。Umemoto和Hirose(2015)认为含1%H的液体外核可以同时符合波速和密度。然而,受配分系数影响,这一组分会导致地幔的H含量超过其饱和上限(Li Y G et al.,2020)。

H可以降低Fe的熔点(Fukai et al.,1982;Sakamaki et al.,2009;Nomura et al.,2014),每增加0.34%的H,Fe的熔点会降低700~900 K(Yuan and Steinle-Neumann,2023)。He等(2022)通过理论模拟发现,H可能以超离子态形式存在于内核中,这种物态的H能够软

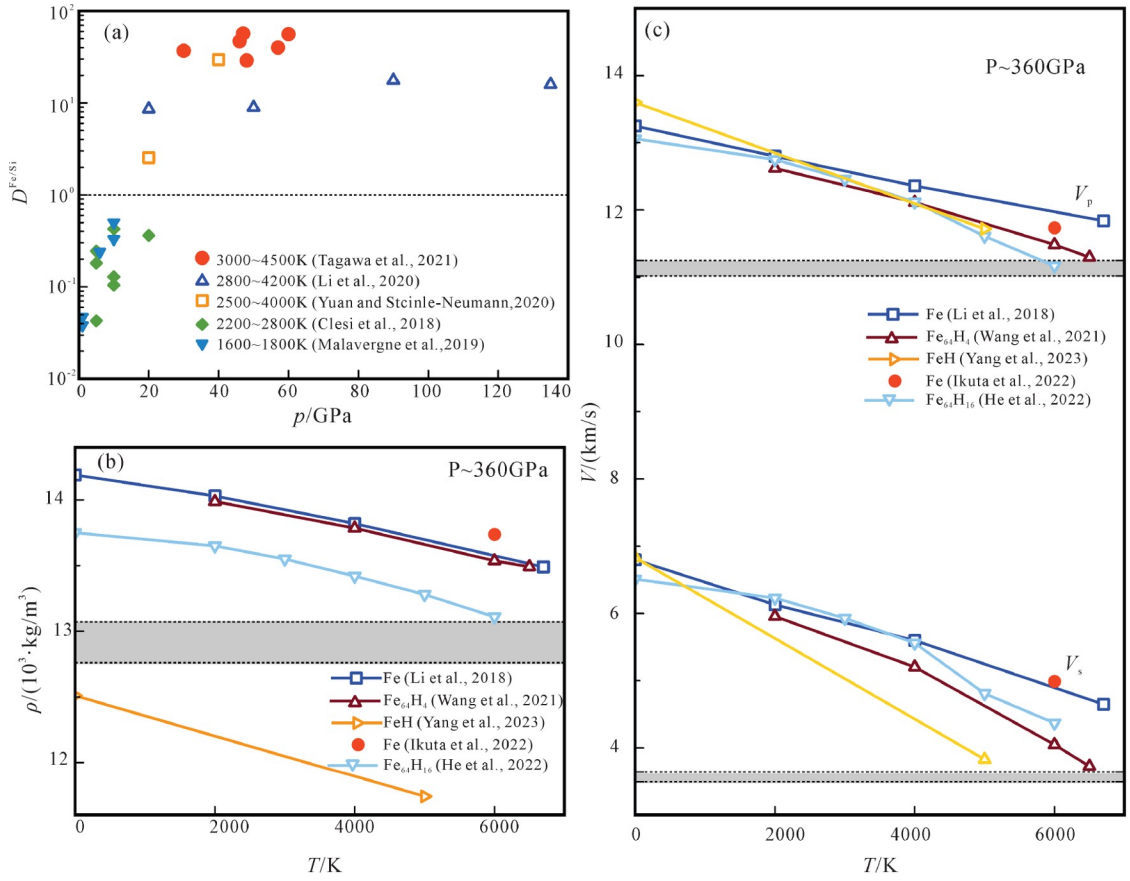

V_S—剪切波速；V_P—压缩波速。(b)(c)灰色区域表示PREM从地心到内外核边界处的密度变化范围

图2 (a)H的金属-硅酸盐配分系数；(b)Fe与Fe-H合金固体密度随温度的变化(修改自Dziewonski and Anderson,1981)；(c)Fe与Fe-H合金固体波速随温度的变化(修改自Dziewonski and Anderson,1981)

Fig.2 (a) Metal-silicate partitioning coefficients of H; (b) Densities of solid Fe and Fe-H alloys as a function of temperature (modified after Dziewonski and Anderson,1981); (c) Sound velocities of solid Fe and Fe-H alloys as a function of temperature (modified after Dziewonski and Anderson,1981)

化内核从而显著降低内核的波速和密度(图2b、2c)。

1.2.2 氧元素 O是地幔中含量最丰富的元素，同时也具有较高的宇宙化学丰度(McDonough and Sun, 1995)。作为亲铁元素，O具有较高的金属-硅酸盐配分系数，能够在核幔分异过程中随金属液滴进入地核(Siebert et al.,2013;Fischer et al.,2015)。O在熔融铁中的溶解度随着压力的增大而显著升高(Takafuji et al.,2005;Sakai et al.,2006)。实验研究表明，在90~140 GPa和3000 K的条件下，熔融铁会与下地幔的钙钛矿$(Mg,Fe)SiO_3$发生化学反应，使O进入熔融地核(Knittle and Jeanloz,1991;Takafuji et al.,2005;Sakai et al.,2006)。因此，O被认为是地核的潜在轻质元素之一。

Rubie等(2015)结合地球增生模拟与金属-硅酸盐配分系数，估算出的地核O含量为2%~4%。Fischer等(2015)通过金刚石对顶砧实验测得O的金属-硅酸盐配分系数，并结合地核密度性质，推测出地核O含量约为1.6%。基于固溶体模型和六方密排结构，不少研究者提出O的内外核配分系数极低(约为0.02)，内核中几乎不含O(<0.1%)(Alfè et al.,2002,2007;Badro et al., 2007;Ozawa et al.,2010)，而外核的O含量则较高(4%~7%)(Alfè et al.,2007;Badro et al.,2007;Frost et al., 2010;Komabayashi,2014;Yokoo et al.,2019;Ichikawa and Tsuchiya,2020)。内外核O含量的巨大差异有助于解释ICB处的密度跳变(Takafuji et al.,2005;Badro et al.,2014;Yokoo et al.,2019)。He等(2022)的理论研究发现，内核条件下O处于超离子态。Liu等(2023)则认为Fe-O系统可能形成特殊的密排结构，导致O进入到内核固体中。这些特殊的结构与物态可能改变O在内外核的配分系数，并对内核的性质产生不可忽略的影响。

当然，也有一些研究者认为O并非外核的主要轻质元素。Tuff等(2011)利用高温高压实验测得Ni、Co等元素的配分系数，通过分析地球增生、氧化和分异过

程,认为要使地幔的Ni、Co等元素达到现在的数值,地核氧含量应为0.15%。Huang等(2011)的冲击波实验证明,Fe-O系统无法同时解释外核的密度和压缩波速(图3)。此外,Komabayashi(2014)利用静态高温高压实验数据计算Fe-O液体的性质,发现O会降低熔融铁的压缩波速,使其偏离外核波速。

此外,O在地核中的含量会随着地核的冷却而改变。如果外核温度足够低,外核顶部的Si与O会结晶形成SiO_2,导致O含量逐渐减少至~1.0%(O'Rourke and Stevenson,2016;Hirose et al.,2017;Zhang Z G et al.,2022)。为了能够同时解释地核的各种性质及其内部的多种现象,需要进一步考虑其他元素与O相互作用的影响(Yokoo et al.,2019;Umemoto and Hirose,2020;Oka et al.,2022;Ichikawa and Tsuchiya,2020)。

1.2.3　*硅元素*　Si作为非挥发性元素,在环境中的扩散能力有限。地幔的Mg/Si值较球粒陨石高,这意味着部分Si可能转移到了地核中(Allègre et al.,1995)。此外,地核含有Si也能解释全硅酸盐地球(Bulk Silicate Earth,BSE)与碳质球粒陨石的$^{30}Si/^{28}Si$值差异(Fitoussi et al.,2009)。Takafuji等(2005)和Sakai等(2006)的实验研究表明,下地幔的(Mg,Fe)SiO_3能与熔融铁发生化学反应,将一定量的Si引入外核。Tuff等(2011)的研究也发现,地核的Si含量达4.3%时可使熔融硅酸盐中的Ni、Co等元素在核幔分异后达到现今地幔的水平。然而,另一些研究则认为,地核中的Si含量可能更高。Rubie等(2015)将多体增生和多步核幔分异模拟相结合,推测出地核的Si含量约为8%~9%。Fischer等(2015)在54 GPa和3350 K下测得Si的金属-硅酸盐配分系数,据此估算出地核的Si含量为8.5%。

假设Si是地核中唯一的轻质元素,在仅考虑密度的情况下,外核液体中的Si含量约为4.5%~12%(Ozawa et al.,2016;Umemoto and Hirose,2020)。然而,外核的Si含量可能受到其他轻质元素的影响。Ozawa等(2016)和Hirose等(2017)发现,O与Si的化学反应能显著降低外核中的Si含量。其他研究也表明,在熔融铁中加入S(Tao and Fei,2021;Sakai et al.,2023)和C(Miozzi et al.,2020;Hasegawa et al.,2021)能够提高Si在内外核中的配分系数,这些元素的存在可能导致外核的Si含量小于3%。

在解释内核性质时,Fe-Si二元合金存在自相矛盾处(图4)。Si能降低固态铁的密度,提高压缩波速并降低剪切波速,Si含量为3%~6%的Fe-Si固溶体的密度和压缩波速与内核一致,但其剪切波速比内核快。若要使剪切波速与内核一致,Si含量需达到9%(即16.4 at.%),这将导致Fe-Si固体的密度过低且压缩波速过高(Lord et al.,2009;Mao et al.,2012;Fischer et al.,2014;Martorell et al.,2016;Antonangeli et al.,2018;Edmund et al.,2019),因此,内核无法简单地近似为Fe-Si二元体系。如果在Fe-Si体系中加入其他轻质元素来降低剪切波速,则有望解决这一矛盾(见1.3小节)。

1.2.4　*硫元素*　地幔中的S含量比陨石低,可能是因为部分S在核幔分离过程中进入了地核,导致地核含1.7%的S(Murthy and Hall,1970;Li et al.,2001;Boujibar et al.,2014)。Boujibar等(2014)探究了1800~2400 K和2~23 GPa条件下S的金属-硅酸盐配分系数,认为S的增生可以发生在地球增生的任何时期。与此不同的是,Suer等(2017)发现高温下S的金属-硅

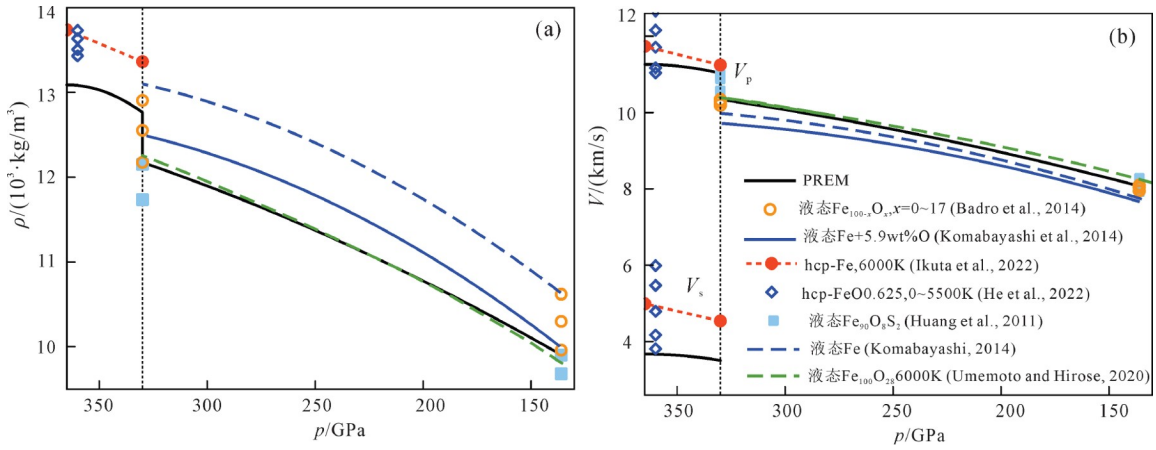

hcp—六方密堆相;V_s—剪切波速;V_p—压缩波速。
黄色中空圆圈由上到下O含量分别为0、2.54%、5.43%;蓝色方块由上到下代表的组分分别为$Fe_{90}O_8S_2$、$Fe_{90}O_{0.5}S_{9.5}$、$Fe_{92.5}O_{2.2}S_{5.3}$;蓝色菱形由上到下代表的温度为3000、4000、5000、5500 K

图3　Fe-O系统的密度与波速随压强的变化(修改自Dziewonski and Anderson,1981)

Fig.3　Densities and sound velocities of Fe-O alloys as a function of pressure(modified after Dziewonski and Anderson,1981)

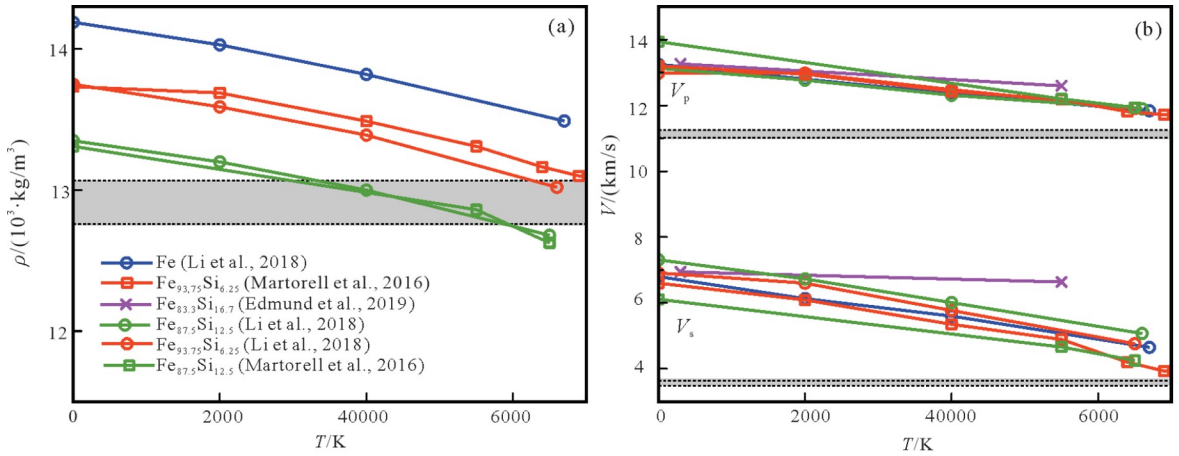

V_s—剪切波速；V_p—压缩波速。灰色区域表示PREM从地心到外核边界处的密度变化范围

图4 Fe-Si系统密度(a)与波速(b)在~360GPa下随温度的变化

Fig.4 Densities (a) and sound velocities (b) of Fe-Si alloys as a function of temperature at pressure of 360 GPa

酸盐配分系数有所降低，S的增生过程很可能发生在地球增生的晚期，他们结合地球化学研究结果，提出地核中的S含量约为2 %。

在仅考虑Fe-S二元合金的情况下，一些实验研究表明外核富含S。如图5b所示，S含量为1.6%的Fe-S合金可以解释外核的密度缺陷(Huang et al.,2011;Kawaguchi et al.,2017;Mori et al.,2017)。然而，Umemoto等(2014)和Badro等(2014)指出，Fe-S液体合金无法同时满足外核的密度和波速约束。图5a展示了通过不同实验数据外推得到的Fe-S系统在内核边界压强下的固液相图。由于对Fe熔点的估算值不同，两张相图的差异较大。尽管如此，这些相图仍能提供一些对Fe-S固液平衡性质的定性描述。Tateno等(2019)和Thompson等(2020,2022)的实验表明，在250 GPa以下，Fe-S合金形成Fe-Fe_3S共晶系统(含16% S)，在250 GPa以上，Fe_3S分解，可能会形成Fe-Fe_2S(含22% S)共晶。但这两种共晶体系均无法结晶出与内核密度相当的固体。相图还表明，无论哪种Fe-S体系，其共晶组分均小于5%~8%，意味着外核的S含量不能超过这一数值，否则外核无法结晶出富Fe的内核。因此，任何组分的Fe-S二元合金都无法完全模拟地核系统。基于Fe-S体系，研究者们还探究了Fe-S-Si和Fe-S-C体系的性质(详见1.3小节)。

1.2.5 *碳元素* C的宇宙化学丰度较高，挥发性强，被认为是地核的潜在轻质元素之一(Wood,1993;Chabot et al.,2006)。Dasgupta等(2013)认为C在低压下具有极强的亲铁性，如果核幔分异时期C弥散在原始大气层或太空中，则地核几乎不含C；反之，如果C溶解在岩浆洋中，地核则可能含有0.2%~1.0%的C。Fischer等(2020)发现，C的亲铁性在高压下有所降低，结合地球的多步增生模型，他们推测地核中的C含量约为0.09%~0.20%。即使占比较低，C仍会对地核的组分和密度产生不可忽略的影响。

Mashino等(2019)由实验数据外推得到330GPa下的Fe-C固液相图(图6a)。如图所示，在ICB条件下，如果Fe-C液体合金的C含量大于3.4%，则系统最有可能结晶出Fe_7C_3(含8.4% C)(Lord et al.,2009;Nakajima et al.,2011;Fei and Brosh,2014;Mashino et al.,2019)。Fe_7C_3固体可以同时满足内核的高泊松比(内核泊松比~0.44，Fe_7C_3泊松比~0.42)和波速(Chen et al.,2014;Prescher et al.,2015)。因此，内核的组分一度被认为是Fe_7C_3。然而，Li等(2016)的研究表明，Fe_7C_3的密度比内核小7.9%。

一些研究者认为，地核中的C大多处于外核中(Lord et al.,2009;Li et al.,2019;Mashino et al.,2019)。在仅考虑Fe-C二元系统的情况下，C含量为0.88%~1.12%的Fe-C液体合金的压缩波速与外核相同，但C含量必须达到2.8%~3.8%才能使其密度与外核一致。因此，C不能作为外核的主要轻质元素(Nakajima et al.,2015)。Mashino等(2019)的熔化实验表明，从常压升高至330 GPa，Fe-C体系的共晶组分从4.3%缓慢降低至3%。如果内核不含C而外核C含量达1.5%~2.0%，则C元素的存在足以解释内外核的密度跳变，再结合其他轻质元素的影响，可能有助于同时解释外核的密度和波速(Li et al.,2019)。

1.2.6 *镍元素* Ni在BSE中的含量比铕(Eu)、钙(Ca)等元素少，这可能是因为部分Ni随金属液滴进入地核成为地核的主要杂质元素(Hirose et al.,2021)。Li和Agee(1996)的实验表明，Ni的亲铁性随压强的升高而降低，当压强外推至~35 GPa时，Ni在金属和硅酸

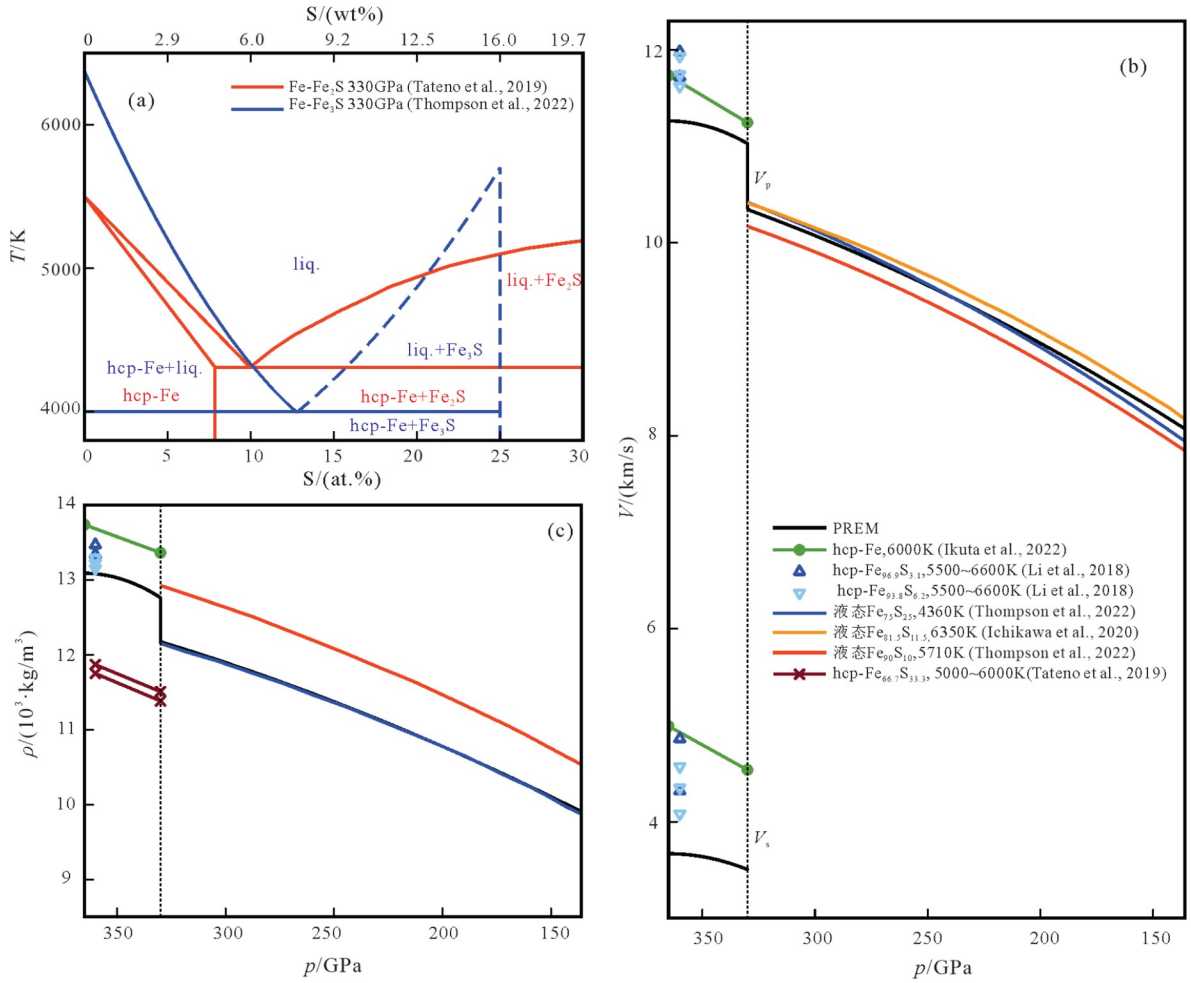

hcp—六方密堆相;liq—液相;V_s—剪切波速;V_p—压缩波速。(a)蓝色虚线表明Fe_3S可能会分解

图5 (a)基于实验数据外推的Fe-Fe_2S和Fe-Fe_3S在330GPa下的相图;(b)Fe-S系统密度随压强的变化关系;(c)Fe-S系统波速随压强的变化关系

Fig.5 (a) Phase diagrams of Fe-Fe_2S and Fe-Fe_3S at pressure of 330 GPa based on the extrapolation of experimental data; (b) Densities of Fe-S alloys as a function of pressure; (c) Sound velocities of Fe-S alloys as a function of pressure

盐中的配分与其地幔丰度相符,据此他们推测核幔分异可能发生在岩浆洋的深部(750~1100 km), 且Ni的金属-硅酸盐配分系数与金属溶体中的Si和O含量有关(Tuff et al.,2011)。

高温高压下Fe与Fe-Ni合金存在六方密堆相(hexagonal close packing,hcp)和面心立方相(face-centered cubic,fcc)的相竞争。图7a展示了不同Ni含量下Fe-Ni合金的相图。纯Fe的hcp-fcc-liquid三相点在90~110 GPa和3000~3500 K处(Jackson et al.,2013;Komabayashi,2014),随着Fe-Ni合金中Ni含量的增加,三相点会向高压方向移动(Lin et al.,2002;Mao et al.,2006;Torchio et al.,2020;Komabayashi,2021)。Zhang等(2016)和Torchio等(2020)认为Ni可能会降低Fe的熔点。然而,Torchio等(2020)指出,即使Ni含量达到36%,Fe-Ni合金的融化曲线也与纯Fe无异。Chatterjee等(2021)的理论计算表明,Fe-Ni合金固溶体的结构稳定性取决于Ni在Fe中的分布情况,当Fe-Ni合金中的Ni原子随机分布时,体心立方相(body-cnetered cubic,bcc)更为稳定。Sun等(2024)的理论模拟也指出,在内核温度压强条件下,Ni会增强bcc相的稳定性。

Ni对Fe的密度和弹性性质只有微小影响(图7b、7c)。Martorell等(2013)的研究表明,Fe-Ni合金的波速与温度密切相关。在低温下,Ni会略微降低Fe的波速,而在360 GPa和5000 K条件下,hcp结构的Fe-Ni波速几乎与Fe一致。

1.3 地核组分预测

单纯考虑二元合金体系难以满足地震学约束,因此,研究者们正在探索三元和更多元的合金体系在地核条件下的密度与波速(表1、2)。例如,Li等(2018)和Wang等(2021)利用第一性原理计算探索了Fe-S-Si、Fe-S-C、Fe-Si-H等系统的波速和密度,发现许多组分

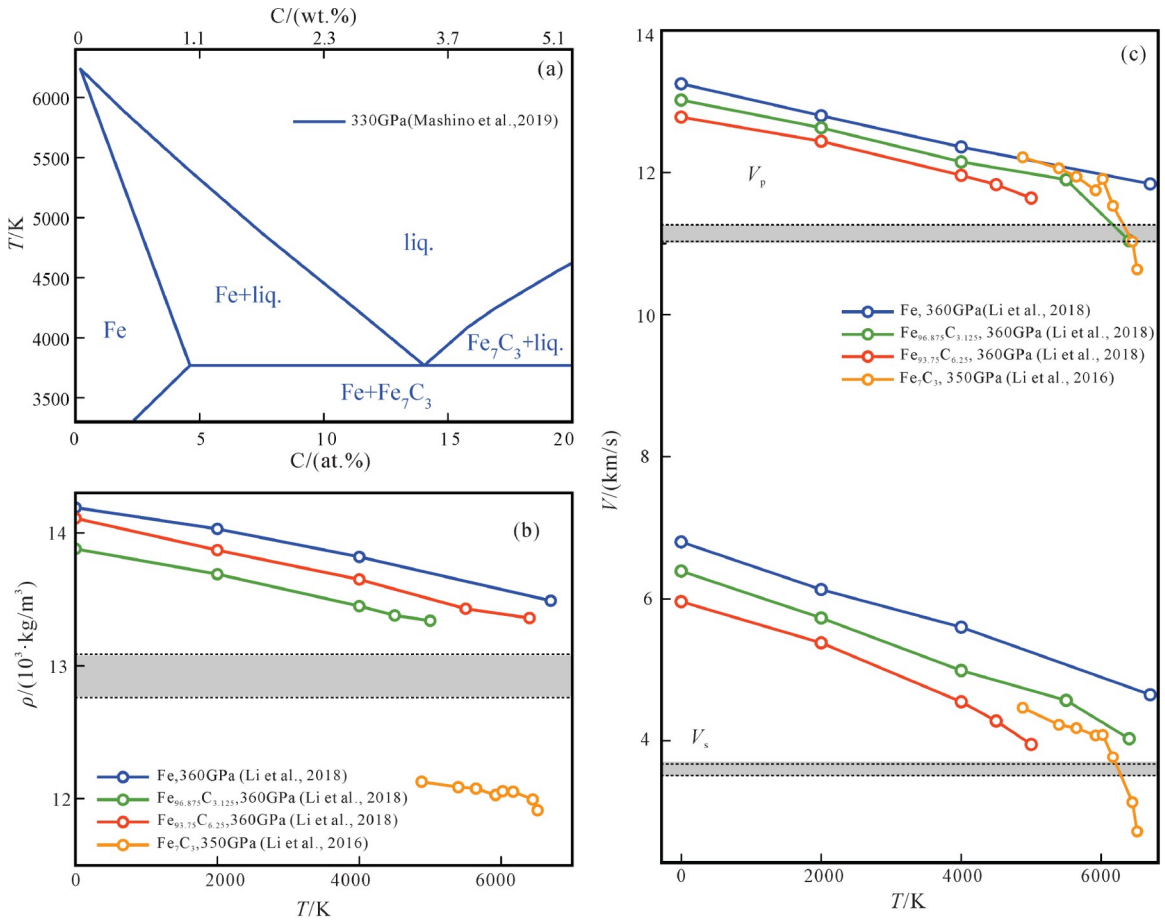

liq—液相；V_s—剪切波速；V_p—压缩波速。灰色区域表示PREM中从地心到外核边界处的密度和波速范围

图6 (a)330 GPa下Fe-C相图(据Mashino et al.,2019)；(b)~360GPa下Fe-C固体的密度与温度关系图；(c)~360GPa下Fe-C固体的波速与温度关系图

Fig.6 (a) Phase diagram of Fe-C alloy at pressurs of 330 GPa (after Mashino et al.,2019); (b) Densities of solid Fe-C alloys as a function of temperature at pressure of 360 GPa; (c) Sound velocities of solid Fe-C alloys as a function of temperature at pressure of 360 GPa

可以同时满足内核的波速和密度约束(图8a、8b)。Sakai等(2023)的实验研究表明，在Fe-S-Si三元合金中，外核中的Si会降低S的内外核配分系数，这意味着如果外核含有大量Si，则S不能成为内核的主要轻质元素。此外，Hasegawa等(2021)的实验指出，Fe-Si-C-S体系在内核条件下无法结晶，内核无法近似为Fe-Si-C-S合金，必须考虑H元素的影响。Umemoto和Hirose(2020)利用第一性原理分子动力学模拟计算了大量Fe合金熔体的密度和波速，并发现了多种能够同时符合地核波速和密度的组分(图8c)。Hirose等(2021)将地球化学对地核组分的估算值与内外核的密度和波速数据相结合，估算了内外核的组分，然而受限于数据，他们的估算未能完全考虑各类轻质元素之间的相互影响和内外核热化学平衡。

当考虑三元或多元体系以及元素相互影响时，地震波数据的约束是不充分的。而且，目前大量针对内核性质的计算都是基于hcp相，对于bcc相或超离子态的研究则较少。因此，构建地核物质的固液相图具有重要意义。这类二元和多元相图能够直接反映固液合金在地核条件下的化学平衡性质以及元素之间的相互影响，全面地展现各类元素在不同晶相和物态下的配分情况，有助于进一步约束地核组分。然而，目前无论是实验还是理论计算，对于地核条件下的Fe合金相图的研究都还比较有限，期待未来有更多的工作深入探究地核物质的固液相图，为确定地核组分提供更多有效约束。

2 内核结构

2.1 内核的各向异性和晶格择优取向

地震波数据不仅反映了地核的密度与波速性质，而且展示了内地核弹性性质的空间各向异性(图9)：

(1)在内核最外层距离ICB约60~100 km处，内核

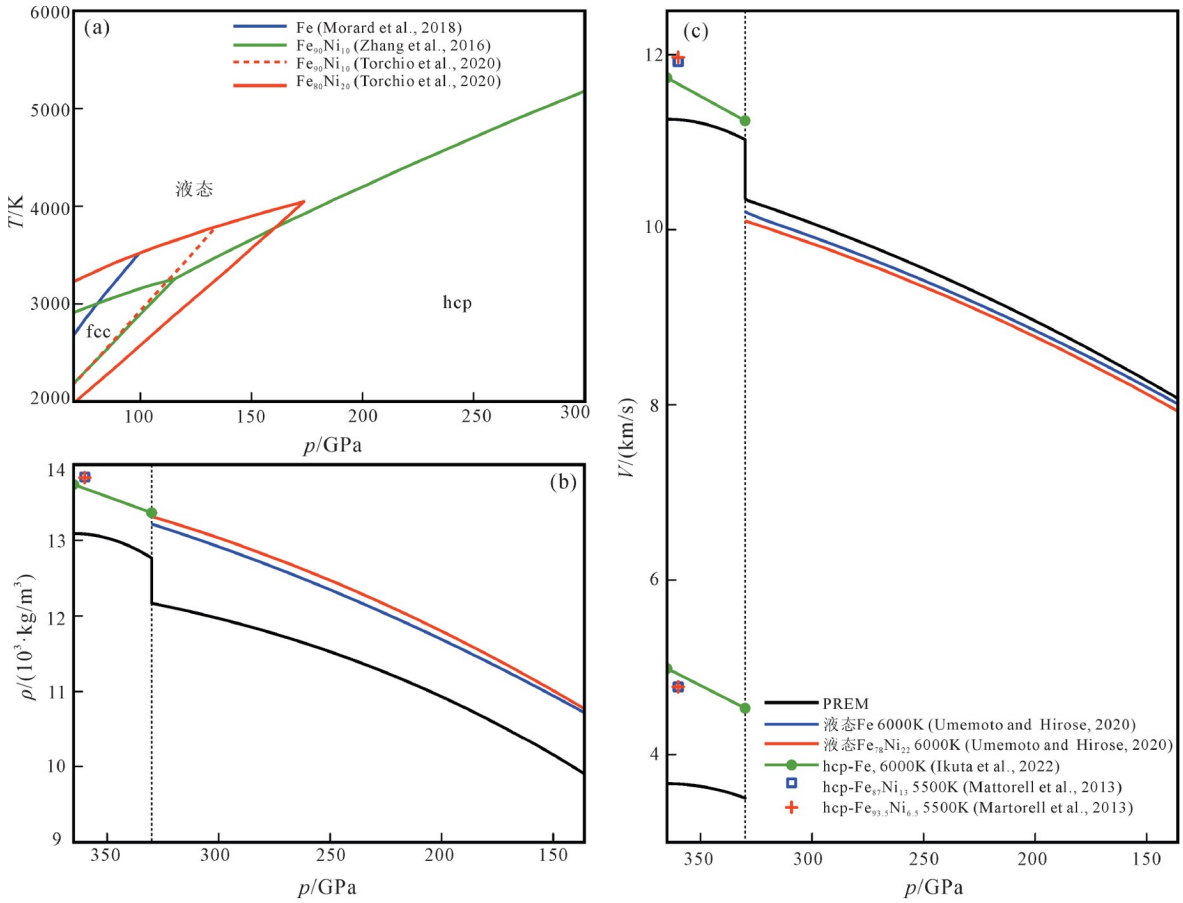

hcp—六方密堆相;fcc—面心立方相;liq—液态;V_s—剪切波速;V_p—压缩波速

图7　(a)Fe-Ni合金相图;(b)Fe-Ni合金的密度与压强变化图;(c)Fe-Ni合金的波速与压强变化图

Fig.7　(a) Phase diagram of Fe-Ni alloys; (b) Densities of Fe-Ni alloys as a function of pressure; (c) Sound velocities of Fe-Ni alloys as a function of pressure

几乎各向同性(各向异性<1%)(Song and Helmberger, 1995a)。ICB附近4~8 km处存在局域泥浆区域(Tian and Wen, 2017);

(2)内核的中间层表现出柱对称的各向异性。该区域沿南北极方向的地震波速度最快且衰减最快,而东西方向(赤道方向)的地震波速度最慢且衰减最慢,南北方向的压缩波速比东西方向的快3%~4%(Morelli et al., 1986);

(3)内核最内层300~650 km区域处的各向异性较为独特。两极方向的地震波速度仍然最快,但是波速最慢的方向与两极方向呈45°~54°角(Ishii and Dziewonski, 2002; Wang and Song, 2018; Stephenson et al., 2021),Pham 和 Tkalčić(2023)称该区域为最内内核(the innermost inner core, IMIC);

(4)东经40° E~160° E的区域被称为准东半球,其余区域被称为准西半球。总体来看,准西半球各向异性更强,地震波衰减更慢,内核最外层波速更慢(Tanaka and Hamaguchi, 1997; Niu and Wen, 2001);

(5)地核中地震波的衰减性随着深度的增加而减小,最内内核中的地震波衰减最弱(Song and Helmberger, 1995b)。

内核地震波速的空间各向异性与内核晶粒结构的不均匀性密切相关。内核中Fe合金晶粒的取向、大小和形状差异造成内核固体排布存在纹理(Pang et al., 2023)。内核的纹理随深度和经度变化,导致了内核独特的异质性和各向异性。内核纹理产生的潜在因素有非匀速生长(Yoshida et al., 1996; Brennan et al., 2021; Sun et al., 2022)、电磁力(Buffett and Wenk, 2001; Ruban et al., 2013; Sun et al., 2023)和枝晶生长(Bergman, 1997; Deguen et al., 2007; Tian and Wen, 2017)。

有研究表明,内核纹理中导致内核波速各向异性的主要因素是晶格择优取向(lattice-preferred orientation, LPO)。晶格择优取向是指部分晶体的晶格朝某一固定方向排列,而剩余晶体的晶格取向则随机分布(Song, 1997)。晶格择优取向的程度随深度而变化且

表 1 部分理论研究地核成分的体系、方法及其对地核中轻质元素含量的推测

Table 1 The system, methods and speculated contents of light elements in the Earth's core in some theoretical studies

体系	方法	内核	外核	参考文献
Fe-O	DFT计算地核条件下体系密度		6.72%~11%	Alfè et al.,1999
Fe-O	DFT探究ICB条件下元素的自由能和内外核配分	0.06%	2.4%	Alfè et al.,2002
Fe-O	DFT探究ICB条件下元素的自由能和内外核配分	0.06%	4.13%	Alfè et al.,2007
Fe-O	DFT计算CMB和ICB条件下体系的密度和波速	地核O含量:3.7%		Badro et al.,2014
Fe-O	利用静态高压实验的数据库计算体系密度、波速和等熵温度梯度		<7.2%~9.1%	Komabayashi,2014
Fe-O	计算体系的密度和波速,结合地幔的元素丰度,确定地核组分	地核O含量:2.7%~5%		Badro et al.,2015
Fe-O-Si-Mg-Al-Ni	理论模拟核幔分异与地球增生过程,计算地核的元素组分	地核O含量:2%~4%		Rubie et al.,2015
Fe-Ni-O	DFT计算外核条件下体系的密度和波速		8%~10%	Umemoto and Hirose,2020
Fe-Ni-O、Fe-O	DFT计算100~450 GPa和4000~8000 K下液体体系的密度和波速,估算地核组分		5.9%~7.4%	Ichikawa and Tsuchiya,2020
Fe-O-Si	DFT计算地核下体系的密度、波速和自由能		1.9%	Zhang Z G et al.,2022
Fe-H	DFT计算100~350 GPa和4000~7000 K下液体系统的密度、压缩波速以及Grüneisen参数		1.0%	Umemoto and Hirose,2015
Fe-Ni-H	DFT计算外核条件下体系的密度和波速		0.8%~1.1%	Umemoto and Hirose,2020
Fe-Ni-H、Fe-H	DFT计算100~450 GPa和4000~8000 K下液体体系密度和波速,通过拟合地学数据确定地核组分		0.62%~0.83%	Ichikawa and Tsuchiya,2020
$MgSiO_3$-Fe-H	DFT计算了H在金属和硅酸盐中的配分系数	地核H含量:1.0%		Yuan Steinle-Neumann,2020
$MgSiO_3$-Fe-H	DFT计算2800~5000 K和135 GPa下H在金属和硅酸盐中的配分系数	地核H含量:<1.0%		Li Y G et al.,2020
Fe-H-Si、Fe-H	DFT计算体系的体弹性模量、剪切模量、密度、剪切波速和压缩波速	0.03%~0.23%		Wang et al.,2021
Fe-H	机器学习+分子动力学模拟计算H的内外核配分系数	0.15%~0.19%	0.31%	Yuan and Steinle-Neumann,2023
Fe-Si	DFT计算ICB条件下Si的自由能和内外核配分系数	4.5%	5.32%	Alfè et al.,2002
Fe-Si	DFT计算ICB条件下Si的自由能和内外核配分系数	3.67%	4.21%	Alfè et al.,2007
Fe-Si	DFT计算CMB和ICB条件下体系的密度和波速	地核Si含量:1.9%		Badro et al.,2014
Fe-Si	计算体系的密度和波速,结合地幔的元素丰度,确定地核组分	地核Si含量:3.6%		Badro et al.,2015
Fe-O-Si-Mg-Al-Ni	理论模拟核幔分异与地球增生过程,计算地核的元素含量	地核Si含量:8%~9%		Rubie et al.,2015
Fe-Si	DFT计算体系在360 GPa下的密度和波速	3.25%		Martorell et al.,2016
Fe–Si	DFT计算体系在360 GPa和0~8000 K下的密度和波速	1.6%		Li et al.,2018
Fe-Ni-Si	DFT计算外核条件下体系的密度和波速		9%~11%	Umemoto and Hirose,2020
Fe-Ni-Si、Fe-Si	DFT计算100~450 GPa和4000~8000 K下液体体系密度和波速,通过拟合地学数据确定地核组分		6.4%~8.7%	Ichikawa and Tsuchiya,2020
Fe-H-Si	DFT计算体系的体弹性模量、剪切模量、密度和波速	3.23%		Wang et al.,2021
Fe-O-Si	DFT计算地核下体系的密度、波速和元素的自由能		1.9%	Zhang Z G et al.,2022
	分析S的挥发性,以及地幔和陨石的S含量差异	1.7%		Murthy and Hall,1970
Fe-S	DFT探究ICB条件下元素的自由能和内外核配分系数	5.08%	6.02%	Alfè et al.,2002
Fe-S	DFT探究ICB条件下元素的自由能和内外核配分系数	4.16%	4.78%	Alfè et al.,2007
Fe-S	DFT计算CMB和ICB条件下体系的密度和波速	地核S含量:<2.4%		Badro et al.,2014
Fe-S	DFT计算150~300 GPa和4000~6000 K下液体体系的密度和压缩波速		14%	Umemoto et al.,2014
Fe-Ni-S	DFT计算外核条件下体系的密度和波速		13%~15%	Umemoto and Hirose,2020
Fe-Ni-S、Fe-S	DFT计算100~450 GPa和4000~8000 K下液体体系密度和波速,通过拟合地学数据确定地核组分		9.6%~11.8%	Ichikawa and Tsuchiya.,2020
Fe-C	DFT计算350 GPa下体系的密度、剪切和压缩波速	8.4%		Li et al.,2016
Fe–C、Fe–Si-C	DFT计算360 GPa和0~8000 K下固体体系的密度、剪切和压缩波速	0.7%~6.3%		Li et al.,2018
Fe-C	DFT计算体系中C的化学势和内外核配分系数		1.5%~2.0%	Li et al.,2019
Fe–C、Fe–Si-C	DFT计算外核条件下液体体系的密度和波速	3.9%~5.1%		Ichikawa and Tsuchiya.,2020

表 2　部分实验研究地核成分的体系、方法及其对地核中轻质元素含量的推测

Table 2　The system, methods and speculated contents of light elements in the Earth's core in some experimental studies

体系	方法	内核	外核	参考文献
(Mg,Fe)SiO_3-Fe-O	在97 GPa 和 3150 K下探究熔融铁合金与钙钛矿的化学反应	实验条件下熔融铁O含量5.3%+Si含量2.8%		Takafuji et al.,2005
(Mg,Fe)SiO_3-Fe-O	在139 GPa和3000 K下探究熔融铁合金与钙钛矿的化学反应		6.3	Sakai et al.,2006
Fe-O	实验测定78 GPa下固体体系的压缩波速	0.1	5.3	Badro et al.,2007
Fe-O	实验探究30~70 GPa和2800~3500 K下O在金属和硅酸盐中的配分特性		6	Frost et al.,2010
Fe-O	DAC实验测定高温高压下体系的相图和密度		7.7	Fischer et al.,2011
Fe-S-O	冲击波实验测定92.6~112.9 GPa下液体体系的体波速		0.5	Huang et al.,2011
Fe-O	实验测定100 GPa和5700 K下O在金属和硅酸盐中的配分特性	地核O含量:1.6% ± 0.3%		Fischer et al.,2015
Fe-O	实验探究150 GPa下Fe-FeO体系的共晶融化关系		>5.0	Morard et al.,2017
Fe-Si-O	实验探究50~140 GPa和3000~4000 K下体系的融化关系		<1.0	Hirose et al.,2017
Fe-S-O	DAC实验探究208 GPa下体系的融化关系,以及元素在内外核中的配分特性		4~5.5	Yokoo et al.,2019
Fe-O-H	DAC实验探究40~150 GPa下体系的液相线		2.9~5.2	Oka et al.,2022
$MgSiO_3$-Fe-H	实验探究7.5 GPa下H在金属和硅酸盐中的配分特性以及与Fe的化学反应	地核H含量:1.23%		Okuchi,1997
Fe-C-H	实验探究127 GPa下体系的融化关系以及H对C溶解度的影响	若外核含H量为1.8 %,则C含量低于0.5%		Hirose et al.,2019
Fe-Si-H	实验探究30~60 GPa和3100~4600 K下H在金属和硅酸盐中的配分特性	地核H含量:0.3%~0.6%		Tagawa et al.,2021
Fe-O-H	实验探究40~150 GPa下体系的液相线关系和H的内外核配分系数	0.03~0.32		Oka et al.,2022
Fe-Si-H	实验探究50 GPa下体系的三元液相线关系和Si、H的内外核配分系数	0.028~0.23	0.04~0.61	Hikosaka et al.,2022
	分析陨石和地幔内的元素比例,据此估算地核组分	地核Si含量:7.3%		Allègre et al.,1995
(Mg,Fe)SiO_3-Fe-O	在139 GPa和3000 K下探究金属合金与钙钛矿的化学反应	地核Si含量:4%		Sakai et al.,2006
Fe-Si	实验测定78 GPa下固体体系的压缩波速	2.3%	2.8%	Badro et al.,2007
	分析陨石的元素丰富度,据此推测地核的组分	地核Si含量:6%		Javoy et al.,2010
Fe-Ni-Si	实验测定0~108 GPa和常温下固体体系的波速	1.2%		Antonangeli et al.,2010
Fe-Si	实验测定98 GPa和300 K下固体体系的压缩波速和密度	8%		Mao et al.,2012
Fe-Ni-Si	实验测定94 GPa和3200 K下液体体系的密度和体弹性模量		2%	Morard et al.,2013
Fe-Si	实验探究145~200 GPa下体系的相图	<4%~9%	<8%~13%	Fischer et al.,2014
Fe-Si	实验探究100 GPa和5700 K下Si在金属和硅酸盐中的配分特性	地核Si含量:8.5% Si		Fischer et al.,2015
Fe-Si	实验探究127 GPa下体系的相图	地核Si含量:<1.5%		Ozawa et al.,2016
Fe-Si-O	实验探究50~140 GPa和3000~4000 K下体系的相图		<0.7%	Hirose et al.,2017
Fe-Si	实验测定140~170 GPa和300 K下固体体系的密度和波速	1%~5%		Antonangeli et al.,2018
Fe-Si	实验测定45~84 GPa和300~1800 K下固体体系的密度和压缩波速	3%~6%		Sakairi et al.,2018
Fe-Si	实验测定110 GPa和2100 K以及0~115 GPa和常温下体系的密度和波速	5%		Edmund et al.,2019
Fe-Si-C	实验探究50~20 GPa下体系的相图和元素的内外核配分系数		0.4%~0.7%	Hasegawa et al.,2021
Fe-Si-H	实验探究50 GPa下体系的三元液相线和Si、H的内外核配分系数	3.24%	3.5%	Hikosaka et al.,2022
Fe-Si-S	实验测定45~189 GPa和1800~4000 K下S、Si的内外核配分系数	2.5%~2.8%	2.7%~3.0%	Sakai et al.,2023
Fe-S	实验测定体系的密度	6%	12%	Sata et al.,2010
Fe-S-O	冲击波实验测定92.6~112.9 GPa下液体体系的体波速		2%~3%	Huang et al.,2011
Fe-Ni-S	实验测定94 GPa和3200 K下液体体系的密度和体弹性模量		6%	Morard et al.,2013
Fe-Si-S	实验探究2 ~23 GPa和1500~2100 K下S在金属和硅酸盐中的配分特性	地核S含量:2%		Boujibar et al.,2014
Fe-S	实验探究34~278 GPa和1600~3500 K下体系的融化特性以及S的内外核配分系数		<6%	Mori et al.,2017
Fe-Ni-S	DAC实验测定体系波速和绝热体模量		5.8%~7.5%	Kawaguchi et al.,2017
Fe-S-O	DAC实验探究208 GPa下体系的融化关系,以及元素的内外核配分特性		0~2%	Yokoo et al.,2019
Fe-S	实验探究306 GPa和3000 K下体系的相图		<5.9%	Tateno et al.,2019
Fe-S	实验测定3126 GPa和2500 K下体系的密度		16%	Thompson et al.,2020

续表2

体系	方法	内核	外核	参考文献
Fe-S	实验测定75 GPa和2800 K下体系的密度、波速、共晶组分和吉布斯自由能等		<8%	Thompson et al.,2022
Fe-Si-S	实验测定45~189 GPa和1800~4000 K下S、Si的内外核配分系数	0.69%~0.70%	1.7%	Sakai et al.,2023
Fe-C	实验探究71.5 GPa和1973 K下体系的密度和热力学稳定性	8.4%		Nakajima et al.,2011
Fe-C	实验探究25 GPa和1473~2073 K下C的内外核配分特性以及体系的相图	8.4%	<2.24%	Fei and Brosh.,2014
Fe-C	实验测定10~53 GPa下固体体系的波速	8.4%		Chen et al.,2014
Fe-C	实验探究70 GPa下液体体系的密度、状态方程和剪切波速		0.88%~3.76%	Nakajima et al.,2015
Fe-C	实验探究205 GPa和3700 K下固体体系的波速	8.4%		Prescher et al.,2015
Fe-C	实验测定150 GPa下体系的共晶融化关系		>2%	Morard et al.,2017
Fe-C-H	实验探究127 GPa下体系的融化关系以及H对C溶解度的影响	若外核含H量为1.8 %，则C<0.5%		Hirose et al.,2019
Fe–C	实验探究255 GPa下体系的共晶融化关系		<3%~4.3%	Mashino et al.,2019
Fe-Si-C	实验探究200 GPa和3000 K下体系的共晶融化关系		<6.6%	Miozzi et al.,2020
Fe-Si-C	实验测定50~20 GPa下体系的相图和元素的内外核配分系数		3.5%~7%	Hasegawa et al.,2021

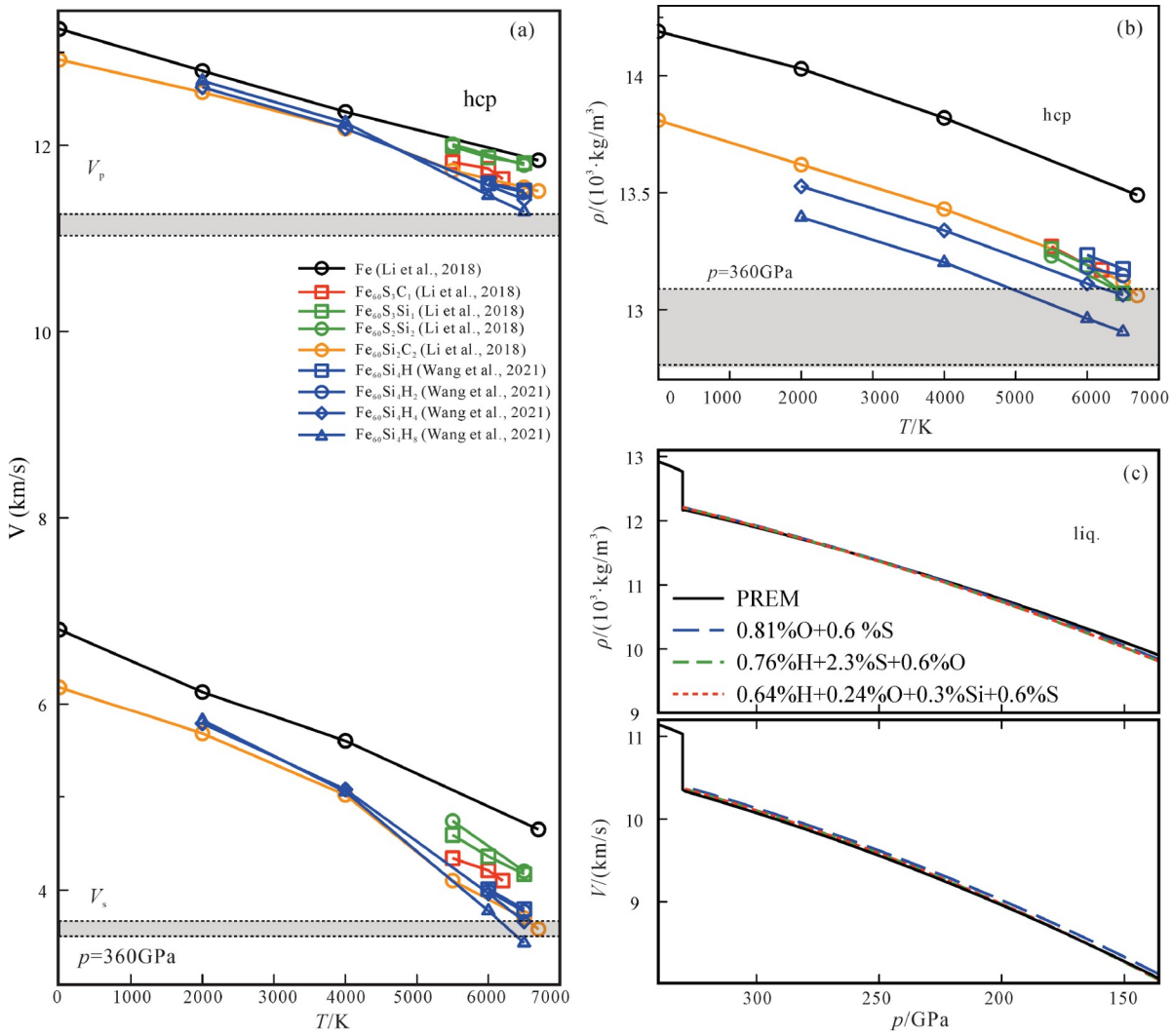

hcp—六方密堆相；liq—液相；V_s—剪切波速；V_p—压缩波速。(c)数据来源：Umemoto and Hirose.,2020

图8 三元Fe合金在~360 GPa下的波速(a)和密度(b)随温度的变化关系；(c)多元Fe合金的波速和密度随压强的变化关系

Fig.8 Densities (a) and sound velocities (b) of ternary alloys as a function of temperature at pressure of 360 GPa; (c) Sound velocities and densities of multi-element alloys as a function of pressure

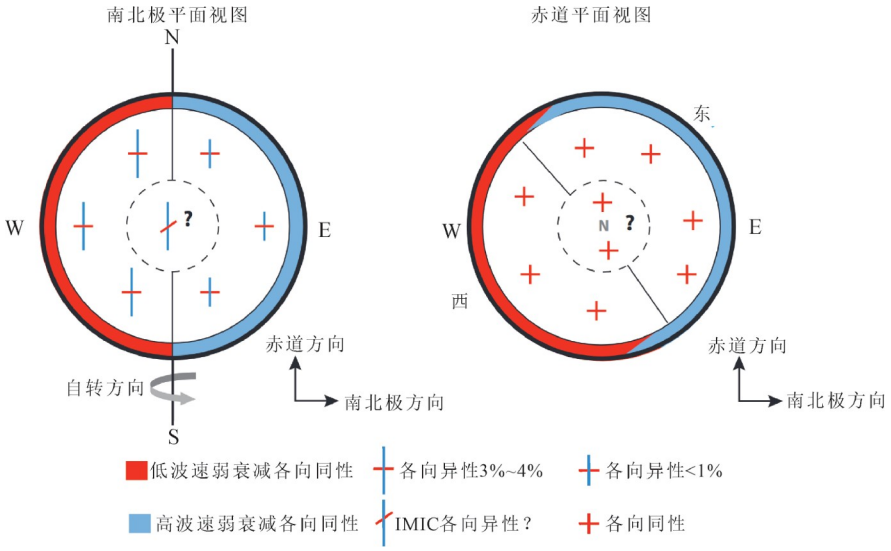

虚线部分表示最内内核 (IMIC) 区域。(a)南北极平面视图;(b)赤道平面视图

图9 内核各向异性示意图(据Deuss,2014修改)

Fig.9 Schematic diagram of the anisotropy of Earth's inner core (modified from Deuss,2014)

存在半球差异,导致内核的各向异性也随深度和经度变化(Sun and Song,2008)。

2.2 内核晶体结构的争议

晶格择优取向对地震波的影响巨大,因此,确定内核的晶体结构至关重要。然而,内核的晶体结构仍存在争议,铁在内核条件下主要可能存在hcp、bcc和fcc三种晶相。由于fcc相在内核条件下的稳定性不如hcp相(Mao et al.,2006;Ekholm et al.,2011;Komabayashi et al.,2012),且fcc结构难以解释内核的各向异性(Stixrude et al.,2009;Mattesini et al.,2010),因此,对内核的晶体结构争议大多数发生在bcc相和hcp相之间。

2.2.1 hcp结构　熔点是决定不同晶相在高温下相对稳定性的重要参量。晶相的熔点越高,热力学稳定性越强。图10a展示了部分研究给出的hcp-Fe和bcc-Fe在地核条件下的熔点。多数研究表明这两种结构的熔点在6000~7000 K之间。由于熔点的精确计算十分困难,且bcc相的高温稳定性受非谐效应影响显著,计算方法的差异可能对结果产生巨大影响,因此hcp和bcc熔点的高低一直存在较大争议。最近,Sun等(2023)和González-Cataldo和Militzer(2023)的研究均表明在地核条件下bcc-Fe的熔点比hcp-Fe低,hcp相更加稳定,但这些研究尚未考虑其他元素对晶相稳定性的影响。

如果内核的晶体结构为hcp且c轴朝向与地球南北极方向一致,则其各向异性就能得到相对合理的解释(Stixrude and Cohen,1995;Steinle-Neumann et al.,2001;Bergman et al.,2010;Tateno et al.,2012;Mäkinen et al.,2014)。然而,不少研究指出hcp-Fe的各向异性与温度关系密切,随着温度升高至内核温度,c/a值会趋于1.63,hcp-Fe将转变为理想hcp晶体,导致其各向异性低于1%(Belonoshko et al.,2003,2008;Vočadlo et al.,2009;Sha and Cohen,2010)。与之不同的是,Modak等(2007)的计算与Sakai等(2011)的实验研究均表明出,内核压强下hcp-Fe的c/a值的温度依赖很弱。Tateno等(2010)通过静态压缩实验测得hcp-Fe在332 GPa和4820 K下的c/a=1.602,远低于理想值1.632。但其实验条件仍然无法直接达到内核的温压范围,因此这一结论需要后续实验的检验。

地震波在地核中传播时会因非弹性效应不断损失能量。hcp-Fe的品质因子高达数十万,是地核品质因子的100倍以上,因此不少研究者认为hcp-Fe无法解释内核对地震波的强衰减效应(Bhattacharyya et al.,1993;Mäkinen et al.,2014;Pejić et al.,2017)。对此,Singh等(2000)提出内核中可能存在3%~10%的液体,增强了hcp-Fe中地震波的能量损耗。此外,Mäkinen等(2014)认为轻质元素对(light element pair)能够增强hcp-Fe合金对地震波的本征损耗。然而,Belonoshko等(2019)指出hcp-Fe中杂质配对的熵过高,严重影响体系的稳定性。

2.2.2 bcc结构　除了hcp相外,内核中铁的另一个主要候选结构是bcc。bcc-Fe在内核条件下的稳定性一直饱受争议。长期以来,不少实验研究通过外推法推断出bcc-Fe在内核条件下不稳定 (Anderson,1986;Steinle-Neumann et al.,2001;Mao et al.,2006)。Dubrovinsky等(2007)首次报道在225 GPa和3400 K下

含10%Ni的Fe-Ni合金发生了从hcp到bcc的相变(图10b)。然而，Tateno等(2012)和Sakai等(2011)通过实验探究了Fe-Ni和Fe-Ni-Si合金的结构性质，均未能复现Dubrovinsky等(2007)的结果。

Vočadlo等(2003)的理论计算指出地核条件下hcp相的热力学稳定性比bcc相更强。然而，Belonoshko等(2011，2017，2022)指出Vočadlo等(2003)的理论计算受到了尺寸效应的制约，当原子数大于1000时，bcc-Fe在内核条件下会发生协同扩散而保持稳定。Ghosh等(2023)在更小尺寸的分子动力学模拟中也观察到了bcc中的固体扩散行为。近期，Zhang等(2023)在hcp固体中也发现了类似的协同扩散行为，并以此解释实验观察到的波速软化现象。

bcc相能够很好地解释内核的波速特征。Belonoshko等(2007)认为bcc结构内的晶粒边界和缺陷会降低剪切模量和剪切波速，从而解释地核较低的硬度和剪切波速。此外，Belonoshko等(2022)通过理论计算表明，在360 GPa和6600 K下，bcc-Fe的剪切波速和压缩波速比hcp-Fe更加接近PREM的地震波速度。如前文所述，最内内核的最快波速方向与最慢方向夹角约为54°。bcc结构的[111]与[100]晶向的夹角非常接近54°。所以bcc相能够解释最内内核独特的各向异性(Belonoshko et al.，2008，2022；Mattesini et al.，2010)。

2.2.3 多相共存 除了单晶结构外，内核也可能是多晶结构的。Mattesini等(2018)提出ICB附近的各向异性是由bcc-hcp多晶的LPO引起的，两种晶体结构的占比影响了各向异性的强度和波速。随着地震波数据的增加，研究者们发现了许多具有局域化各向异性的内核区域，简单的柱对称模型难以完全解释内核各区域的各向异性(Zhang B et al.，2023)。因此，内核中的晶体结构可能是复杂的多晶共存。这一观点得到了实验

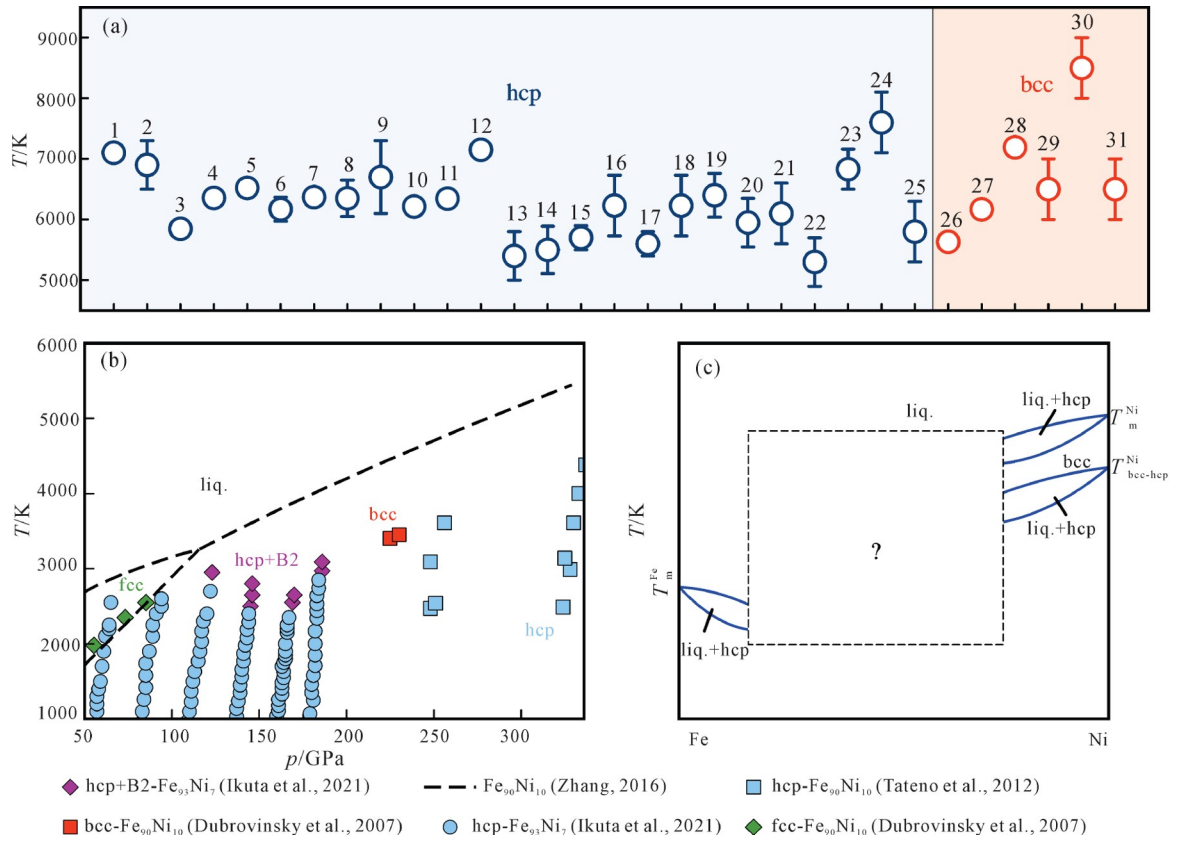

hcp—六方密堆相；bcc—体心立方相；fcc—面心立方相；B2—有序的bcc相；liq—液相；V_s—剪切波速；V_p—压缩波速；T^{Ni}_m—Ni的熔点；T^{Fe}_m—Fe的熔点；$T^{Ni}_{bcc\text{-}hcp}$—Ni的bcc和hcp转变温度；(c)问号表示此区域可能存在hcp-bcc共存。(a)数据来源：Yuan，2023；Sola，2009；Sun，2023；González-Cataldo and Militzer，2023；Sun，2018；Alfè et al.，1999，2002，2009；Davies，2019；Zhang，2015；Belonoshko，2000；Laio et al.，2000；Sinmyo，2019；Zhang，2016；Anzelini，2013；Murphy，2011；Kraus，2022；Turneaure，2020；Li J et al.，2020；Nguyen，2004；Ahrens，2002；Y00，1993；Williams，1987；Brown，1986；Sun，2023；Belonoshko，2021；Bouchet，2013；Morard，2011

图10 (a)hcp-Fe和bcc-Fe在地核条件下的熔点；(b)Fe-Ni结构相图；(c)根据现有研究推测的地核条件下的Fe-Ni相图(据Sun et al.，2024)

Fig.10 (a) The melting temperatures of the hcp-Fe and bcc-Fe under Earth's core condition; (b) Phase diagram of Fe-Ni; and (c) A "likely" phase diagram of Fe-Ni (modified from Sun et al.，2024)

支持。Ikuta等(2021)发现Fe-Ni合金在高温高压下存在hcp-B2共存相(B2为有序的bcc相),且Ni和Si的存在会增大hcp-B2相共存的稳定范围,在两相混合状态下,固体系统的密度和压缩波速更加符合PREM的数值。

Sun等(2022)模拟研究发现,在内核形核与生长的过程中,由于hcp相的形核能垒过高,Fe可能会发生两步相变过程,即液态Fe先形成bcc相再形成hcp相。而Ni的加入会使Fe合金更易于形成hcp-bcc共存结构(Sun et al.,2024)。但精确的共晶组分极大地依赖地核条件下的Fe-Ni相图,这需要后续更多的研究去验证(图10c)。

2.2.4　超离子态　He等(2022)的理论模拟发现,在330~360 GPa和2500~3500 K下,C、H和O原子会在hcp-Fe中呈现超离子态。这些原子像液体一样在Fe晶格的间隙处流动,具有较高的扩散系数和离子电导率。Sun等(2023)还发现,hcp-Fe中H原子沿c轴方向扩散的能垒最低,在外磁场的作用下,Fe-H晶体的c轴朝向会倾向于与磁场方向平行,该效应会增强内核中hcp-Fe的LPO,从而解释内核的各向异性。此外,超离子态原子对地核条件下Fe合金的性质具有显著影响。理论计算表明,处于超离子态的轻质元素会降低Fe的剪切波速和压缩波速,使其更加接近PREM的波速(Wang et al.,2021;He et al.,2022;Yang et al.,2023)。此外,超离子态原子可能改变铁-轻质元素相图,这需要后续更多的研究去探索。

3　内核形核

3.1　地核演化与地磁场关联

地磁场阻挡了太阳风和宇宙射线,是地球宜居性的必要条件。地球发电机模型能够解释地磁场与地核活动的关系(Gubbins,1977;Lister and Buffett,1995;Labrosse et al.,2001;Labrosse,2015)。该模型认为,外地核能够将来自内核的能量转为地磁场的能量,并向地幔散热。地球发电机模型提供了一个清晰的物理图像,即地磁场强度会受到内核冷却与生长、外核的冷却与热传导、地核中放射性元素的衰变、地核的组分变化以及地核的温度分布等多种因素影响。

地磁场与地核的演化紧密相关,而且与内核冷却及生长的关系尤为密切。根据地球发电机模型估算出内核的年龄约为5~15亿年(Labrosse et al.,2001;Labrosse,2015;Nimmo,2015;Driscoll and Davies,2023)。地核物质的热导率数值存在较大争议,导致内核年龄具有极大的不确定性。一些研究认为核幔边界处的物质热导率较低,约为30~50 W m^{-1} K^{-1}(Stacey and Anderson,2001;Stacey and Loper,2007;Basu et al.,2020)。然而,也有不少理论和实验工作认为核幔边界热导率远高于此,约为70~250 W m^{-1} K^{-1}(Pozzo et al.,2012,2022;Zhang Y J et al.,2022)。但古地磁研究表明,地磁场的年龄可能为30~40亿年(Tarduno et al.,2010;Bono et al.,2022),即内核的年龄应小于地磁场的年龄。在内核形成之前,地磁场主要依靠液核的冷却散热来维持。然而,Driscoll和Davies(2023)和Olson(2013)认为如果地核物质的热导率较高,则地核散热无法维持地磁场,这一问题被称为新地核悖论(The new core paradox)。为了解释这一悖论,研究者们提出在内核形成之前地球发动机可能存在其他的能量来源,例如外核顶部的Fe-Si-O系统会结晶出SiO_2并释放重力势能,为早期的地磁场提供能量(Hirose et al.,2017;Wilson et al.,2022)。

3.2　传统形核理论与内地核形核悖论

从目前所知的地核内部演化历史来看,地核最初是熔融的液体,在温度降低到一定程度后才逐渐结晶出固态内核。一般认为,当地核熔体温度低于其熔点便可以结晶(Jacobs,1953;Nimmo,2015)。然而,根据经典形核理论(Classical Nucleation Theory,CNT),均质液体只有形成一定大小的临界晶核后才能发生大规模结晶。由于固液界面的存在,形成晶核需要克服吉布斯自由能垒,这不但大大延长了形核所需的时间,而且还要求液体形核时的温度低于熔点,即过冷(Christian,2002)。CNT的这些观点也得到了理论和实验的证实(Shibuta et al.,2017;Kelton and Greer,2010)。

Huguet等(2018)认为,如果早期地核内部不存在固体,则内地核的形成过程应遵循经典形核理论,那么地核的形核也可以为内核年龄提供约束。临界晶核形成之后,内核的生长主要分为两个阶段。初始阶段内核在过冷环境中迅速生长,其生长速率取决于外核物质的扩散速率(Huguet et al.,2016)。当内核生长到一定大小后,内外核边界处的温度接近熔点,内核生长受到自身散热的制约,生长速率放缓。Huguet等(2018)的计算结果表明,假设内地核的形核等待时间为10亿年,则地核所需的过冷度约为–1000 K。早期的研究表明,地核温度每10亿年降低100 K(Nimmo,2015),这意味着地核不可能在地球的年龄范围内冷却到形核所需的过冷度。Huguet等(2018)将这个问题称为内地核形核悖论(Earth′s inner core nucleation paradox)。Lasbleis等(2020)发现在内核的快速生长阶段,一些液体物质会被困在内核中,假设内核的液体含量不超过10%,则内核形核的过冷度不能超过–100K。

近年来,许多工作探究了地核的形核过程,图11a

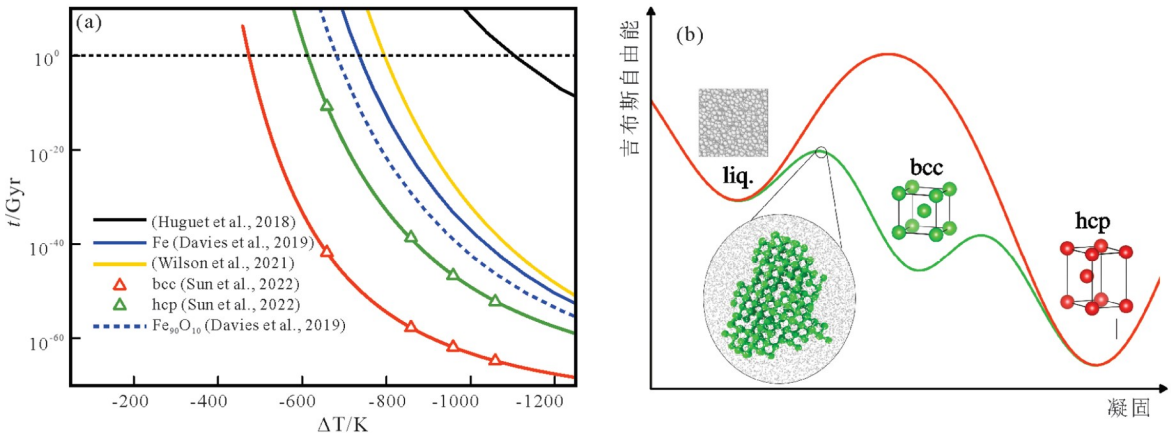

hcp—六方密堆相；bcc—体心立方相；liq—液相。(a)黑色虚线表示时间为10亿年；(b)红线表示传统形核过程，绿线表示两步形核过程

图11 (a)内地核形核等待时间与过冷度关系图；(b)内地核形核过程液体-bcc-hcp的两步形核机理图(据Sun et al.，2022)

Fig.11 (a) The waiting time of the Earth's inner core nucleation as a function of cooling temperature; (b) Schematic diagram of two-step nucleation of the Earth's inner core (modified from Sun et al., 2022)

展示了形核等待时间与过冷度的关系。Davies等(2019)利用半经验势函数模拟了Fe和Fe-O系统的形核过程，并估算出这些体系在323 GPa下形核所需的过冷度分别为–730 K和–675 K。Sun等(2022)通过永胚法(persistent-embryo method)和分子动力学模拟计算了bcc-Fe和hcp-Fe的形核速率，发现bcc-Fe的形核速率比hcp-Fe高几十个数量级。这意味着内核会先形成亚稳的bcc相，然后再相变为稳定的hcp相。如图11b所示，内核的两步形核机制可以显著降低形核所需过冷度，有助于解决内地核形核悖论。Wilson等(2021，2023)的计算结果表明，Si和S会提高形核所需过冷度，而O和C能够将过冷度降低至–600~–730 K。这些研究得到的形核所需过冷度仍高于合理数值。内核的形核过程与地核物质结构、物态以及化学成分密切相关，内核形核悖论仍然是一个有待解决的难题。

4 结语

本文回顾了近年来关于地球内外核成分、内核晶体结构与形核的研究进展。目前，富Fe的二元合金体系无法很好地解释内外地核的波速和密度。虽然一些三元和多元合金体系能够满足地震学约束，但轻质元素之间的相互作用以及固液热平衡所应满足的热力学和化学约束尚不明确。此外，内核物质的微观结构与纹理对于理解内核波速的各向异性极为重要，但内核晶体结构仍存在较大争议。内核中的一些轻质元素可能处于超离子态，这类物态对化学成分以及内核晶相竞争的影响尚不明确。内核物质的晶体结构与元素在内外核中的配分会互相影响，因此，发展地核物质的固液相图对于全面理解地核成分与结构具有重要意义。外核冷却散热和内核结晶生长与地磁场的演变历史密切关联。然而，地核演化过程中仍存在诸如“新地核悖论”和“内地核形核悖论”等谜团。未来需要更多的实验和理论模拟工作推进对地球内外核的组分、结构以及演化过程的研究。

作者贡献声明： 高宸，数据收集和整理、稿件撰写、图件制作；Kai-Ming Ho，文章讨论、修改；孙阳，研究构思和设计、文章撰写与修订。

利益冲突声明： 作者保证本文无利益冲突。

致谢： 感谢审稿专家对本文提出的宝贵意见！

参考文献 (References):

Ahrens T J, Holland K G, Chen G Q. 2002. Phase diagram of iron, revised-core temperatures. Geophysical Research Letters, 29(7): 54–1

Alfè D, Gillan M J, Price G D. 2002. Composition and temperature of the Earth's core constrained by combining ab initio calculations and seismic data. Earth and Planetary Science Letters, 195(1–2): 91–98

Alfè D, Gillan M J, Price G D. 2007. Temperature and composition of the Earth's core. Contemporary Physics, 48(2): 63–80

Alfè D, Price G D, Gillan M J. 1999. Oxygen in the Earth's core: A first-principles study. Physics of the Earth and Planetary Interiors, 110(3–4): 191–210

Alfè D. 2009. Temperature of the inner-core boundary of the Earth: Melting of iron at high pressure from first-principles coexistence simulations. Physical Review B, 79(6): 060101

Allègre C J, Poirier J P, Humler E, Hofmann A W. 1995. The chemical composition of the Earth. Earth and Planetary Science Letters, 134(3): 515–526

Anderson O L. 1986. Properties of iron at the Earth's core conditions. Geophysical Journal International, 84(3): 561–579

Anderson W W, Ahrens T J. 1994. An equation of state for liquid iron and

implications for the Earth's core. Journal of Geophysical Research: Solid Earth, 99(B3): 4273–4284

Antonangeli D, Morard G, Paolasini L, Garbarino G, Murphy C A, Edmund E, Decremps F, Fiquet G, Bosak A, Mezouar M, Fei Y W. 2018. Sound velocities and density measurements of solid hcp-Fe and hcp-Fe-Si (9 wt.%) alloy at high pressure: Constraints on the Si abundance in the Earth's inner core. Earth and Planetary Science Letters, 482: 446–453

Antonangeli D, Siebert J, Badro J, Farber D L, Fiquet G, Morard G, Ryerson F J. 2010. Composition of the Earth's inner core from high-pressure sound velocity measurements in Fe-Ni-Si alloys. Earth and Planetary Science Letters, 295(1–2): 292–296

Anzellini S, Dewaele A, Mezouar M, Loubeyre P, Morard G. 2013. Melting of iron at Earth's inner core boundary based on fast X-ray diffraction. Science, 340(6131): 464–466

Badro J, Brodholt J P, Piet H, Siebert J, Ryerson F J. 2015. Core formation and core composition from coupled geochemical and geophysical constraints. Proceedings of the National Academy of Sciences of the United States of America, 112(40): 12310f12314

Badro J, Côté A S, Brodholt J P. 2014. A seismologically consistent compositional model of Earth's core. Proceedings of the National Academy of Sciences of the United States of America, 111(21): 7542–7545

Badro J, Fiquet G, Guyot F, Gregoryanz E, Occelli F, Antonangeli D, d'Astuto M. 2007. Effect of light elements on the sound velocities in solid iron: Implications for the composition of Earth's core. Earth and Planetary Science Letters, 254(1–2): 233–238

Basu A, Field M R, McCulloch D G, Boehler R. 2020. New measurement of melting and thermal conductivity of iron close to outer core conditions. Geoscience Frontiers, 11(2): 565f568

Belonoshko A B, Ahuja R, Johansson B. 2000. Quasi–ab initio molecular dynamic study of Fe melting. Physical Review Letters, 84(16): 3638

Belonoshko A B, Ahuja R, Johansson B. 2003. Stability of the body-centred-cubic phase of iron in the Earth's inner core. Nature, 424(6952): 1032–1034

Belonoshko A B, Arapan S, Rosengren A. 2011. An ab initio molecular dynamics study of iron phases at high pressure and temperature. Journal of Physics Condensed Matter: an Institute of Physics Journal, 23(48): 485402

Belonoshko A B, Fu J, Bryk T, Simak S I, Mattesini M. 2019. Low viscosity of the Earth's inner core. Nature Communicaitons, 10(1): 2483

Belonoshko A B, Fu J, Smirnov G. 2021. Free energies of iron phases at high pressure and temperature: Molecular dynamics study. Physical Review B, 104(10): 104103

Belonoshko A B, Lukinov T, Fu J, Zhao J J, Davis S, Simak S I. 2017. Stabilization of body-centred cubic iron under inner-core conditions. Nature Geoscience, 10: 312–316

Belonoshko A B, Simak S I, Olovsson W, Vekilova O Y. 2022. Elastic properties of body-centered cubic iron in Earth's inner core. Physical Review B, 105(18): L180102

Belonoshko A B, Skorodumova N V, Davis S, Osiptsov A N, Rosengren A, Johansson B. 2007. Origin of the low rigidity of the Earth's inner core. Science, 316(5831): 1603–1605

Belonoshko A B, Skorodumova N V, Rosengren A, Johansson B. 2008. Elastic anisotropy of Earth's inner core. Science, 319(5864): 797–800

Bergman M I, Lewis D J, Myint I H, Slivka L, Karato S I, Abreu A. 2010. Grain growth and loss of texture during annealing of alloys, and the translation of Earth's inner core. Geophysical Research Letters, 37(22): L22313

Bergman M I. 1997. Measurements of electric anisotropy due to solidification texturing and the implications for the Earth's inner core. Nature, 389: 60–63

Bhattacharyya J, Shearer P, Masters G. 1993. Inner core attenuation from short-period PKP(BC) versus PKP(DF) waveforms. Geophysical Journal International, 114(1): 1–11

Birch F. 1952. Elasticity and constitution of the Earth's interior. Journal of Geophysical Research, 57(2): 227–286

Bono R K, Paterson G A, Boon A, Engbers Y A, Michael Grappone J, Handford B, Hawkins L M A, Lloyd S J, Sprain C J, Thallner D, Biggin A J. 2022. The PINT database: A definitive compilation of absolute palaeomagnetic intensity determinations since 4 billion years ago. Geophysical Journal International, 229(1): 522–545

Bouchet J, Mazevet S, Morard G, Guyot F, Musella R. 2013. Ab initio equation of state of iron up to 1500 GPa. Physical Review B, 87(9): 094102

Boujibar A, Andrault D, Bouhifd M A, Bolfan-Casanova N, Devidal J L, Trcera N. 2014. Metal-silicate partitioning of sulphur, new experimental and thermodynamic constraints on planetary accretion. Earth and Planetary Science Letters, 391: 42–54

Brennan M C, Fischer R A, Couper S, Miyagi L, Antonangeli D, Morard G. 2021. High-pressure deformation of iron-nickel-silicon alloys and implications for earth's inner core. Journal of Geophysical Research: Solid Earth, 126(3): e2020JB021077

Brown J M, McQueen R G. 1986. Phase transitions, Grüneisen parameter, and elasticity for shocked iron between 77 GPa and 400 GPa. Journal of Geophysical Research: Solid Earth, 91(B7): 7485–7494

Buffett B A, Wenk H R. 2001. Texturing of the Earth's inner core by Maxwell stresses. Nature, 413(6851): 60–63

Chabot N L, Campbell A J, Jones J H, Humayun M, Lauer H V J. 2006. The influence of carbon on trace element partitioning behavior. Geochimica et Cosmochimica Acta, 70(5): 1322–1335

Chatterjee S, Ghosh S, Saha-Dasgupta T. 2021. Ni doping: A viable route to make body-centered-cubic Fe stable at earth's inner core. Minerals, 11(3): 258

Chen B, Li Z Y, Zhang D Z, Liu J C, Hu M Y, Zhao J Y, Bi W L, Alp E E, Xiao Y M, Chow P, Li J. 2014. Hidden carbon in Earth's inner core revealed by shear softening in dense Fe_7C_3. Proceedings of the National Academy of Sciences of the United States of America, 111(50): 17755–17758

Christian J. 2002. The theory of transformations in metals and alloys. Newnes: Pergamon, 422–461

Clesi V, Bouhifd M A, Bolfan-Casanova N, Manthilake G, Schiavi F, Raepsaet C, Bureau H, Khodja H, Andrault D. 2018. Low hydrogen contents in the cores of terrestrial planets. Science Advances, 4(3): e1701876

Dasgupta R, Chi H, Shimizu N, Buono, A S, Walker D. 2013. Carbon solution and partitioning between metallic and silicate melts in a shallow magma ocean: Implications for the origin and distribution of terrestrial carbon. Geochimica et Cosmochimica Acta, 102: 191–212.

Davies C J, Pozzo M, Alfè D. 2019. Assessing the inner core nucleation paradox with atomic-scale simulations. Earth and Planetary Science Letters, 507: 1–9

Deguen R, Alboussière T, Brito D. 2007. On the existence and structure of a mush at the inner core boundary of the Earth. Physics of the Earth and Planetary Interiors, 164(1–2): 36–49

Deuss A. 2014. Heterogeneity and anisotropy of earth's inner core. Annual Review of Earth and Planetary Sciences, 42: 103–126

Driscoll P, Davies C. 2023. The "new core paradox": Challenges and potential solutions. Journal of Geophysical Research: Solid Earth, 128(1): e2022JB025355

Dubrovinsky L, Dubrovinskaia N, Narygina O, Kantor I, Kuznetzov A, Prakapenka V B, Vitos L, Johansson B, Mikhaylushkin A S, Simak S I, Abrikosov I A. 2007. Body-centered cubic iron-nickel alloy in Earth's core. Science, 316(5833): 1880–1883

Dziewonski A M, Anderson D L. 1981. Preliminary reference Earth model. Physics of the Earth and Planetary Interiors, 25(4): 297–356

Edmund E, Antonangeli D, Decremps F, Miozzi F, Morard G, Boulard E, Clark A N, Ayrinhac S, Gauthier M, Morand M, Mezouar M. 2019. Velocity-density systematics of Fe-5wt%Si: Constraints on Si content in the earth's inner core. Journal of Geophysical Research: Solid Earth, 124 (4): 3436–3447

Ekholm M, Mikhaylushkin A, Simak S, Johansson B, Abrikosov I. 2011. Configurational thermodynamics of Fe-Ni alloys at Earth's core conditions. Earth and Planetary Science Letters, 308(1): 90–96

Fei Y W, Brosh E. 2014. Experimental study and thermodynamic calculations of phase relations in the Fe-C system at high pressure. Earth and Planetary Science Letters, 408: 155–162

Fiquet G, Auzende A L, Siebert J, Corgne A, Bureau H, Ozawa H, Garbarino G. 2010. Melting of peridotite to 140 gigapascals. Science, 329(5998): 1516–1518

Fischer R A, Campbell A J, Caracas R, Reaman D M, Heinz D L, Dera P, Prakapenka V B. 2014. Equations of state in the Fe-FeSi system at high pressures and temperatures. Journal of Geophysical Research: Solid Earth, 119(4): 2810–2827

Fischer R A, Campbell A J, Shofner G A, Lord O T, Dera P, Prakapenka V B. 2011. Equation of state and phase diagram of FeO. Earth and Planetary Science Letters, 304(3–4): 496–502

Fischer R A, Cottrell E, Hauri E, Lee K K M, Le V M. 2020. The carbon content of Earth and its core. Proceedings of the National Academy of Sciences of the United States of America, 117(16): 8743–8749.

Fischer R A, Nakajima Y, Campbell A J, Frost D J, Harries D, Langenhorst F, Miyajima N, Pollok K, Rubie D C. 2015. High pressure metal-silicate partitioning of Ni, Co, V, Cr, Si, and O. Geochimica et Cosmochimica Acta, 167: 177–194

Fitoussi C, Bourdon B, Kleine T, Oberli F, Reynolds B C. 2009. Si isotope systematics of meteorites and terrestrial peridotites: Implications for Mg/Si fractionation in the solar nebula and for Si in the Earth's core. Earth and Planetary Science Letters, 287(1–2): 77–85

Frost D J, Asahara Y, Rubie D C, Miyajima N, Dubrovinsky L S, Holzapfel C, Ohtani E, Miyahara M, Sakai T. 2010. Partitioning of oxygen between the Earth's mantle and core. Journal of Geophysical Research: Solid Earth, 115(B2): 2009JB006302

Fukai Y, Fukizawa A, Watanabe K, Amano M. 1982. Hydrogen in iron-its enhanced dissolution under pressure and stabilization of the γ phase. Japanese Journal of Applied Physics, 21(5A): L318

Ghosh M, Zhang S, Hu L M, Hu S X. 2023. Cooperative diffusion in body-centered cubic iron in Earth and super-Earths' inner core conditions. Journal of Physics: Condensed Matter, 35(15):154002

González-Cataldo F, Militzer B. 2023. Ab initio determination of iron melting at terapascal pressures and Super-Earths core crystallization. Physical Review Research, 5(3): 033194

Gubbins D. 1977. Energetics of the Earth's Core. Journal of Geophysics, 43 (1): 453–464

Halliday A N, Wood B J. 2009. How did earth accrete? Science, 325(5936): 44–45

Hasegawa M, Hirose K, Oka K, Ohishi Y. 2021. Liquidus phase relations and solid-liquid partitioning in the Fe-Si-C system under core pressures. Geophysical Research Letters, 48(13): e2021GL092681

He Y, Sun S C, Kim D Y, Jang B G, Li H P, Mao H K. 2022. Superionic iron alloys and their seismic velocities in Earth's inner core. Nature, 602 (7896): 258–262

Hikosaka K, Tagawa S, Hirose K, Okuda Y, Oka K, Umemoto K, Ohishi Y. 2022. Melting phase relations in Fe-Si-H at high pressure and implications for Earth's inner core crystallization. Scientific Reports, 12 (1): 10000

Hirose K, Morard G, Sinmyo R, Umemoto K, Hernlund J, Helffrich G, Labrosse S. 2017. Crystallization of silicon dioxide and compositional evolution of the Earth's core. Nature, 543(7643): 99–102

Hirose K, Tagawa S, Kuwayama Y, Sinmyo R, Morard G, Ohishi Y, Genda H. 2019. Hydrogen limits carbon in liquid iron. Geophysical Research Letters, 46(10): 5190–5197

Hirose K, Wood B, Vočadlo L. 2021. Light elements in the Earth's core. Nature Reviews Earth & Environment, 2: 645–658

Huang H J, Fei Y W, Cai L C, Jing F Q, Hu X J, Xie H S, Zhang L M, Gong Z Z. 2011. Evidence for an oxygen-depleted liquid outer core of the Earth. Nature, 479(7374): 513–516

Huguet L, Alboussière T, Bergman M I, Deguen R, Labrosse S, Lesœur G. 2016. Structure of a mushy layer under hypergravity with implications for Earth's inner core. Geophysical Journal International, 204(3): 1729–1755

Huguet L, Orman J A V, Hauck S A, Willard M A. 2018. Earth's inner core nucleation paradox. Earth and Planetary Science Letters, 487: 9–20

Ichikawa H, Tsuchiya T, Tange Y. 2014. The *P-V-T* equation of state and thermodynamic properties of liquid iron. Journal of Geophysical Research: Solid Earth, 119(1): 240–252

Ichikawa H, Tsuchiya T. 2020. Ab initio thermoelasticity of liquid iron-nickel-light element alloys. Minerals, 10(1): 59

Iizuka-Oku R, Yagi T, Gotou H, Okuchi T, Hattori T, Sano-Furukawa A. 2017. Hydrogenation of iron in the early stage of Earth's evolution. Nature Communications, 8: 14096

Ikuta D, Ohtani E, Fukui H, Sakai T, Ishikawa D, Baron A Q R. 2022. Sound velocity of hexagonal close-packed iron to the Earth's inner core pressure. Nature Communications, 13(1): 7211

Ikuta D, Ohtani E, Hirao N. 2021. Two-phase mixture of iron-nickel-silicon alloys in the Earth's inner core. Communications Earth & Environment, 2: 225

Ishii M, Dziewoński A M. 2002. The innermost inner core of the earth: Evidence for a change in anisotropic behavior at the radius of about 300 km. Proceedings of the National Academy of Sciences of the United States of America, 99(22): 14026–14030

Jackson J M, Sturhahn W, Lerche M, Zhao J Y, Toellner T S, Alp E E, Sinogeikin S V, Bass J D, Murphy C A, Wicks J K. 2013. Melting of compressed iron by monitoring atomic dynamics. Earth and Planetary Science Letters, 362: 143–150

Jacobs J A. 1953. The Earth's inner core. Nature, 172: 297–298

Javoy M, Kaminski E, Guyot F, Andrault D, Sanloup C, Moreira M, Labrosse S, Jambon A, Agrinier P, Davaille A, Jaupart C. 2010. The chemical composition of the Earth: Enstatite chondrite models. Earth and Planetary Science Letters, 293(3–4): 259–268

Kawaguchi S I, Nakajima Y, Hirose K, Komabayashi T, Ozawa H, Tateno S, Kuwayama Y, Tsutsui S, Baron A Q R. 2017. Sound velocity of liquid Fe-Ni-S at high pressure. Journal of Geophysical Research: Solid Earth, 122 (5): 3624–3634

Kelton K F, Greer A L. 2010. Nucleation in Condensed Matter: Applications in Materials and Biology. Amsterdam: Elsevier: 165–226

Knittle E, Jeanloz R. 1991. The high-pressure phase diagram of $Fe_{0.94}O$: A possible constituent of the Earth's core. Journal of Geophysical Research: Solid Earth, 96(B10): 16169–16180

Komabayashi T, Hirose K, Ohishi Y. 2012. In situ X-ray diffraction measurements of the fcc-hcp phase transition boundary of an Fe-Ni alloy in an internally heated diamond anvil cell. Physics and Chemistry of Minerals, 39(4): 329–338

Komabayashi T. 2014. Thermodynamics of melting relations in the system Fe-FeO at high pressure: Implications for oxygen in the Earth's core. Journal of Geophysical Research: Solid Earth, 119(5): 4164–4177

Komabayashi T. 2021. Phase relations of Earth's core-forming materials. Crystals, 11(6): 581

Kraus R G, Hemley R J, Ali S J, Belof J L, Benedict L X, Bernier J, Braun D, Cohen R E, Collins G W, Coppari F, Desjarlais M P, Fratanduono P, Hamel S, Krygier A, Lazicki A, Mcnaney J, Millot M, Myint P C, Newman M G, Rygg J R, Sterbentz D M, Stewart S T, Stixrude L, Swift D C, Wehrenberg C, Eggert J H. 2022. Measuring the melting curve of iron at super-Earth core conditions. Science, 375(6577): 202–205

Labrosse S, Poirier J P, Le Mouël J L. 2001. The age of the inner core. Earth and Planetary Science Letters, 190(3–4): 111–123

Labrosse S. 2015. Thermal evolution of the core with a high thermal conductivity. Physics of the Earth and Planetary Interiors, 247: 36–55

Laio A, Bernard S, Chiarotti G L, Scandolo S, Tosatti E, 2000. Physics of Iron at Earth's Core Conditions. Science, 287(5455): 1027–1030

Lasbleis M, Kervazo M, Choblet G. 2020. The fate of liquids trapped during the Earth's inner core growth. Geophysical Research Letters, 47(2): e2019GL085654

Li J, Agee C B. 1996. Geochemistry of mantle–core differentiation at high pressure. Nature, 381(6584): 686–689

Li J, Fei Y, Mao H K, Hirose K, Shieh S R. 2001. Sulfur in the Earth's inner core. Earth and Planetary Science Letters. 193(3–4): 509–514

Li J, Fei Y. 2014. Treatise on Geochemistry. Amsterdam: Elsevier, 527–557

Li J, Wu Q, Li J, Xue T, Tan Y, Zhou X, Zhang Y, Xiong Z W, Gao Z P, Sekine T. 2020a. Shock melting curve of iron: A consensus on the temperature at the Earth′s inner core boundary. Geophysical Research Letters, 47(15): e2020GL087758

Li Y G, Vočadlo L, Alfè D, Brodholt J. 2019. Carbon partitioning between the earth's inner and outer core. Journal of Geophysical Research: Solid Earth, 124(12): 12812–12824

Li Y G, Vočadlo L, Brodholt J, Wood I G. 2016. Thermoelasticity of Fe_7C_3 under inner core conditions. Journal of Geophysical Research: Solid Earth, 121(8): 5828–5837

Li Y G, Vočadlo L, Brodholt J. 2018. The elastic properties of hcp-Fe alloys under the conditions of the Earth's inner core. Earth and Planetary Science Letters, 493: 118–127

Li Y G, Vočadlo L, Sun T, Brodholt J P. 2020. The Earth's core as a reservoir of water. Nature Geoscience, 13: 453–458

Lin J F, Heinz D L, Campbell A J, Devine J M, Mao W L, Shen G Y. 2002. Iron-Nickel alloy in the Earth's core. Geophysical Research Letters, 29 (10): 1471

Lister J R, Buffett B A. 1995. The strength and efficiency of thermal and compositional convection in the geodynamo. Physics of the Earth and Planetary Interiors, 91(1–3): 17–30

Liu J, Sun Y, Lv C J, Zhang F, Fu S Y, Prakapenka V B, Wang C Z, Ho K, Lin J, Wentzcovitch R M. 2023. Iron-rich Fe-O compounds at Earth's core pressures. The Innovation, 4(1): 100354

Lord O T, Walter M J, Dasgupta R, Walker D, Clark S M. 2009. Melting in the Fe-C system to 70GPa. Earth and Planetary Science Letters, 284(1–2): 157–167

Mäkinen A M, Deuss A, Redfern S A T. 2014. Anisotropy of Earth's inner core intrinsic attenuation from seismic normal mode models. Earth and Planetary Science Letters, 404: 354–364

Malavergne V, Bureau H, Raepsaet C, Gaillard F, Poncet M, Surblé S, Sifré D, Shcheka S, Fourdrin C, Deldicque D, Khodja H. 2019. Experimental constraints on the fate of H and C during planetary core-mantle differentiation. Implications for the Earth. Icarus, 321: 473–485

Mao W L, Campbell A J, Heinz D L, Shen G Y. 2006. Phase relations of Fe-Ni alloys at high pressure and temperature. Physics of the Earth and Planetary Interiors, 155(1–2): 146–151

Mao Z, Lin J F, Liu J, Alatas A, Gao L L, Zhao J Y, Mao H K. 2012. Sound velocities of Fe and Fe-Si alloy in the Earth's core. Proceedings of the National Academy of Sciences of the United States of America, 109(26): 10239–10244

Martorell B, Brodholt J, Wood I G, Vočadlo L. 2013. The effect of nickel on the properties of iron at the conditions of Earth's inner core: Ab initio calculations of seismic wave velocities of Fe-Ni alloys. Earth and Planetary Science Letters, 365: 143–151

Martorell B, Wood I G, Brodholt J, Vočadlo L. 2016. The elastic properties of hcp-$Fe_{1-x}Si_x$ at Earth's inner-core conditions. Earth and Planetary Science Letters, 451: 89–96

Mashino I, Miozzi F, Hirose K, Morard G, Sinmyo R. 2019. Melting experiments on the Fe-C binary system up to 255 GPa: Constraints on the carbon content in the Earth's core. Earth and Planetary Science Letters, 515: 135–144

Mattesini M, Belonoshko A B, Buforn E, Ramírez M, Simak S I, Udías A, Mao H K, Ahuja R. 2010. Hemispherical anisotropic patterns of the Earth's inner core. Proceedings of the National Academy of Sciences of

the United States of America, 107(21): 9507–9512

Mattesini M, Belonoshko A B, Tkalčić H. 2018. Polymorphic nature of iron and degree of lattice preferred orientation beneath the earth's inner core boundary. Geochemistry, Geophysics, Geosystems, 19(1): 292–304

McDonough W F, Sun S S. 1995. The composition of the Earth. Chemical Geology, 120(3–4): 223–253

Miozzi F, Morard G, Antonangeli D, Baron M A, Boccato S, Pakhomova A, Garbarino G, Mezouar M, Fiquet G. 2020. Eutectic melting of Fe-3 at% Si-4 at% C up to 200 GPa and implications for the Earth's core. Earth and Planetary Science Letters, 544: 116382

Modak P, Verma A K, Rao R S, Godwal B K, Stixrude L, Jeanloz R. 2007. Stability of the hcp phase and temperature variation of the axial ratio of iron near Earth-core conditions. Journal of Physics: Condensed Matter, 19 (1): 016208

Morard G, Andrault D, Antonangeli D, Nakajima Y, Auzende A L, Boulard E, Cervera S, Clark A, Lord O T, Siebert J, Svitlyk V, Garbarino G, Mezouar M. 2017. Fe-FeO and Fe-Fe_3C melting relations at Earth's core-mantle boundary conditions: Implications for a volatile-rich or oxygen-rich core. Earth and Planetary Science Letters, 473: 94–103

Morard G, Boccato S, Rosa A D, Anzellini S, Miozzi F, Henry L, Garbarino G, Mezouar M, Harmand M, Guyot F, Boulard E, Kantor I, Irifune T, Torchio R. 2018. Solving Controversies on the Iron Phase Diagram Under High Pressure. Geophysical Research Letters, 45(20): 11–074

Morard G, Bouchet J, Valencia D, Mazevet S, Guyot F. 2011. The melting curve of iron at extreme pressures: Implications for planetary cores. High Energy Density Physics, 7(3): 141–144

Morard G, Siebert J, Andrault D, Guignot N, Garbarino G, Guyot F, Antonangeli D. 2013. The Earth's core composition from high pressure density measurements of liquid iron alloys. Earth and Planetary Science Letters, 373: 169–178

Morelli A, Dziewonski A M, Woodhouse J H. 1986. Anisotropy of the inner core inferred from PKIKP travel times. Geophysical Research Letters, 13 (13): 1545–1548

Mori Y, Ozawa H, Hirose K, Sinmyo R, Tateno S, Morard G, Ohishi Y. 2017. Melting experiments on Fe-Fe_3S system to 254 GPa. Earth and Planetary Science Letters, 464: 135–141

Murphy C A, Jackson J M, Sturhahn W, Chen B. 2011. Melting and thermal pressure of hcp-Fe from the phonon density of states. Physics of the Earth and Planetary Interiors, 188(1–2): 114–120

Murthy V R, Hall H T. 1970. The chemical composition of the Earth's core: Possibility of sulphur in the core. Physics of the Earth and Planetary Interiors, 2(4): 276–282

Nakajima Y, Imada S, Hirose K, Komabayashi T, Ozawa H, Tateno S, Tsutsui S, Kuwayama Y, Baron A Q R. 2015. Carbon-depleted outer core revealed by sound velocity measurements of liquid iron-carbon alloy. Nature Communications, 6: 8942

Nakajima Y, Takahashi E, Sata N, Nishihara Y, Hirose K, Funakoshi K I, Ohishi Y. 2011. Thermoelastic property and high-pressure stability of Fe_7C_3: Implication for iron-carbide in the Earth's core. American Mineralogist, 96(7): 1158–1165

Nguyen J H, Holmes N C. 2004. Melting of iron at the physical conditions of the Earth′s core. Nature, 427(6972): 339–342

Nimmo F. 2015. Energetics of the core. Treatise on Geophysics. 8: 27–55

Niu F, Wen L. 2001. Hemispherical variations in seismic velocity at the top of the Earth's inner core. Nature, 410(6832): 1081–1084

Nomura R, Hirose K, Uesugi K, Ohishi Y, Tsuchiyama A, Miyake A, Ueno Y. 2014. Low core-mantle boundary temperature inferred from the solidus of pyrolite. Science, 343(6170): 522–525

O'Rourke J G, Stevenson D J. 2016. Powering Earth's dynamo with magnesium precipitation from the core. Nature, 529(7586): 387–389

Oka K, Ikuta N, Tagawa S, Hirose K, Ohishi Y. 2022. Melting experiments on Fe-O-H and Fe-H: Evidence for eutectic melting in Fe-FeH and implications for hydrogen in the core. Geophysical Research Letters, 49 (17): e2022GL099420

Okuchi T. 1997. Hydrogen partitioning into molten iron at high pressure: Implications for Earth's core. Science, 278(5344): 1781–1784

Olson P. 2013. The new core paradox. Science, 342(6157): 431–432

Ozawa H, Hirose K, Tateno S, Sata N, Ohishi Y. 2010. Phase transition boundary between B1 and B8 structures of FeO up to 210 GPa. Physics of the Earth and Planetary Interiors, 179(3–4): 157–163

Ozawa H, Hirose K, Yonemitsu K, Ohishi Y. 2016. High-pressure melting experiments on Fe-Si alloys and implications for silicon as a light element in the core. Earth and Planetary Science Letters, 456: 47–54

Pang G N, Koper K D, Wu S M, Wang W, Lasbleis M, Euler G. 2023. Enhanced inner core fine-scale heterogeneity towards Earth's centre. Nature, 620(7974): 570–575

Pejić T, Tkalčić H, Sambridge M, Cormier V F, Benavente R. 2017. Attenuation tomography of the upper inner core. Journal of Geophysical Research: Solid Earth, 122(4): 3008–3032

Pham T S, Tkalčić H. 2023. Up-to-fivefold reverberating waves through the Earth's center and distinctly anisotropic innermost inner core. Nature Communications, 14(1): 754

Poirier J P. 1994. Light elements in the Earth's outer core: A critical review. Physics of the Earth and Planetary Interiors, 85(3–4): 319–337

Pozzo M, Davies C J, Dario A. 2022. Towards reconciling experimental and computational determinations of Earth's core thermal conductivity. Earth and Planetary Science Letters, 584: 117466

Pozzo M, Davies C, Gubbins D, Alfè D. 2012. Thermal and electrical conductivity of iron at Earth's core conditions. Nature, 485(7398): 355–358

Prescher C, Dubrovinsky L, Bykova E, Kupenko I, Glazyrin K, Kantor A, McCammon C, Mookherjee M, Nakajima Y, Miyajima N, Sinmyo R, Cerantola V, Dubrovinskaia N, Prakapenka V, Rüffer R, Chumakov A, Hanfland M. 2015. High Poisson's ratio of Earth's inner core explained by carbon alloying. Nature Geoscience, 8: 220–223

Ruban A V, Belonoshko A B, Skorodumova N V. 2013. Impact of magnetism on Fe under Earth's core conditions. Physical Review B, 87: 014405

Rubie D C, Jacobson S A, Morbidelli A, O'Brien D P, Young E D, de Vries J, Nimmo F, Palme H, Frost D J. 2015. Accretion and differentiation of the terrestrial planets with implications for the compositions of early-formed Solar System bodies and accretion of water. Icarus, 248: 89–108

Sakai F, Hirose K, Morard G. 2023. Partitioning of silicon and sulfur between solid and liquid iron under core pressures: Constraints on Earth's core composition. Earth and Planetary Science Letters, 624: 118449

Sakai T, Kondo T, Ohtani E, Terasaki H, Endo N, Kuba T, Suzuki T, Kikegawa T. 2006. Interaction between iron and post-perovskite at core-mantle

boundary and core signature in plume source region. Geophysical Research Letters, 33(15): 2006GL026868

Sakai T, Ohtani E, Hirao N, Ohishi Y. 2011. Stability field of the hcp-structure for Fe, Fe-Ni, and Fe-Ni-Si alloys up to 3 Mbar. Geophysical Research Letters, 38(9): 2011GL047178

Sakairi T, Sakamaki T, Ohtani E, Fukui H, Kamada S, Tsutsui S, Uchiyama H, Baron A Q R. 2018. Sound velocity measurements of hcp Fe-Si alloy at high pressure and high temperature by inelastic X-ray scattering. American Mineralogist, 103(1): 85–90

Sakamaki K, Takahashi E, Nakajima Y, Nishihara Y, Funakoshi K, Suzuki T, Fukai Y. 2009. Melting phase relation of FeH up to 20 GPa: Implication for the temperature of the Earth's core. Physics of the Earth and Planetary Interiors, 174(1–4): 192–201

Sakamaki T, Ohtani E, Fukui H, Kamada S, Takahashi S, Sakairi T, Takahata A, Sakai T, Tsutsui S, Ishikawa D, Shiraishi R, Seto Y, Tsuchiya T, Baron A Q R. 2016. Constraints on Earth's inner core composition inferred from measurements of the sound velocity of hcp-iron in extreme conditions. Science Advances, 2(2): e1500802

Sata N, Hirose K, Shen G Y, Nakajima Y, Ohishi Y, Hirao N. 2010. Compression of FeSi, Fe_3C, $Fe_{0.95}O$, and FeS under the core pressures and implication for light element in the Earth's core. Journal of Geophysical Research: Solid Earth, 115(B9): 2009JB006975

Sha X W, Cohen R E. 2010. Elastic isotropy of -Fe under Earth's core conditions. Geophysical Research Letters, 37(10): 2009GL042224

Shibuta Y, Sakane S, Miyoshi E, Okita S, Takaki T, Ohno M. 2017. Heterogeneity in homogeneous nucleation from billion-atom molecular dynamics simulation of solidification of pure metal. Nature Communications, 8(1): 10

Siebert J, Badro J, Antonangeli D, Ryerson F J. 2013. Terrestrial accretion under oxidizing conditions. Science, 339(6124): 1194–1197

Singh S C, Taylor M A J, Montagner J P. 2000. On the presence of liquid in Earth's inner core. Science, 287(5462): 2471–2474

Sinmyo R, Hirose K, Ohishi Y. 2019. Melting curve of iron to 290 GPa determined in a resistance-heated diamond-anvil cell. Earth and Planetary Science Letters, 510: 45–52

Sola E, Alfe D. 2009. Melting of Iron under Earth's Core Conditions from Diffusion Monte Carlo Free Energy Calculations. Physical Review Letters, 103(7): 078501

Song X D, Helmberger D V. 1995a. Depth dependence of anisotropy of Earth's inner core. Journal of Geophysical Research: Solid Earth, 100(B6): 9805–9816

Song X D, Helmberger D V. 1995b. A P wave velocity model of Earth's core. Journal of Geophysical Research: Solid Earth, 100(B6): 9817–9830

Song X D. 1997. Anisotropy of the Earth's inner core. Reviews of Geophysics, 35(3): 297–313

Stacey F D, Anderson O L. 2001. Electrical and thermal conductivities of Fe-Ni-Si alloy under core conditions. Physics of the Earth and Planetary Interiors, 124(3–4): 153–162

Stacey F D, Loper D E. 2007. A revised estimate of the conductivity of iron alloy at high pressure and implications for the core energy balance. Physics of the Earth and Planetary Interiors, 161(1–2): 13–18

Steinle-Neumann G, Stixrude L, Cohen R E, Gülseren O. 2001. Elasticity of iron at the temperature of the Earth's inner core. Nature, 413(6851): 57–60

Stephenson J, Tkalčić H, Sambridge M. 2021. Evidence for the innermost inner core: Robust parameter search for radially varying anisotropy using the neighborhood algorithm. Journal of Geophysical Research: Solid Earth, 126(1): e2020JB020545

Stixrude L, Cohen R E. 1995. High-pressure elasticity of iron and anisotropy of earth's inner core. Science, 267(5206): 1972–1975

Stixrude L, de Koker N, Sun N, Mookherjee M, Karki B B. 2009. Thermodynamics of silicate liquids in the deep Earth. Earth and Planetary Science Letters, 278(3–4): 226–232

Suer T A, Siebert J, Remusat L, Menguy N, Fiquet G. 2017. A sulfur-poor terrestrial core inferred from metal-silicate partitioning experiments. Earth and Planetary Science Letters, 469: 84–97.

Sun S C, He Y, Yang J Y, Lin Y F, Li J F, Kim D Y, Li H P, Mao H K. 2023. Superionic effect and anisotropic texture in Earth's inner core driven by geomagnetic field. Nature Communications, 14(1): 1656

Sun T, Brodholt J P, Li Y, Vočadlo L. 2018. Melting properties from ab initio free energy calculations: Iron at the Earth′s inner-core boundary. Physical Review B, 98(22): 224301

Sun X L, Song X D. 2008. The inner inner core of the Earth: Texturing of iron crystals from three-dimensional seismic anisotropy. Earth and Planetary Science Letters, 269(1–2): 56–65

Sun Y, Mendelev M I, Zhang F, Liu X, Da B, Wang C Z, Wentzcovitch R M, Ho K M. 2024. Unveiling the effect of Ni on the formation and structure of Earth's inner core. Proceedings of the National Academy of Sciences of the United States of America, 121(4): e2316477121

Sun Y, Zhang F, Mendelev M I, Wentzcovitch R M, Ho K M. 2022. Two-step nucleation of the Earth's inner core. Proceedings of the National Academy of Sciences of the United States of America, 119(2): e2113059119

Tagawa S, Sakamoto N, Hirose K, Yokoo S, Hernlund J, Ohishi Y, Yurimoto H. 2021. Experimental evidence for hydrogen incorporation into Earth's core. Nature Communications, 12(1): 2588

Takafuji N, Hirose K, Mitome M, Bando Y. 2005. Solubilities of O and Si in liquid iron in equilibrium with (Mg, Fe)SiO_3 perovskite and the light elements in the core. Geophysical Research Letters, 32(6): 2005GL022773

Tanaka S, Hamaguchi H. 1997. Degree one heterogeneity and hemispherical variation of anisotropy in the inner core from PKP(BC)-PKP(DF) times. Journal of Geophysical Research: Solid Earth, 102(B2): 2925–2938

Tao R B, Fei Y W. 2021. High-pressure experimental constraints of partitioning behavior of Si and S at the Mercury's inner core boundary. Earth and Planetary Science Letters, 562: 116849

Tarduno J A, Cottrell R D, Watkeys M K, Hofmann A, Doubrovine P V, Mamajek E E, Liu D J, Sibeck D G, Neukirch L P, Usui Y. 2010. Geodynamo, solar wind, and magnetopause 3.4 to 3.45 billion years ago. Science, 327(5970): 1238–1240

Tateno S, Hirose K, Komabayashi T, Ozawa H, Ohishi Y. 2012. The structure of Fe-Ni alloy in Earth's inner core. Geophysical Research Letters, 39 (12): 2012GL052103

Tateno S, Hirose K, Ohishi Y, Tatsumi Y. 2010. The structure of iron in Earth's inner core. Science, 330(6002): 359–361

Tateno S, Ozawa H, Hirose K, Suzuki T, I-Kawaguchi S, Hirao N. 2019. Fe_2S: The most Fe-rich iron sulfide at the earth's inner core pressures.

Geophysical Research Letters, 46(21): 11944–11949

Thompson S, Komabayashi T, Breton H, Suehiro S, Glazyrin K, Pakhomova A, Ohishi Y. 2020. Compression experiments to 126 GPa and 2500 K and thermal equation of state of Fe_3S: Implications for sulphur in the Earth's core. Earth and Planetary Science Letters, 534: 116080

Thompson S, Sugimura-Komabayashi E, Komabayashi T, McGuire C, Breton H, Suehiro S, Ohishi Y. 2022. High-pressure melting experiments of Fe_3S and a thermodynamic model of the Fe-S liquids for the Earth's core. Journal of Physics: Condensed Matter, 34(39): 394003

Tian D D, Wen L X. 2017. Seismological evidence for a localized mushy zone at the Earth's inner core boundary. Nature Communications, 8(1): 165

Torchio R, Boccato S, Miozzi F, Rosa A D, Ishimatsu N, Kantor I, Sévelin-Radiguet N, Briggs R, Meneghini C, Irifune T, Morard G. 2020. Melting curve and phase relations of Fe-Ni alloys: Implications for the earth's core composition. Geophysical Research Letters, 47(14): e2020GL088169

Tuff J, Wood B J, Wade J. 2011. The effect of Si on metal-silicate partitioning of siderophile elements and implications for the conditions of core formation. Geochimica et Cosmochimica Acta, 75(2): 673–690

Turneaure S J, Sharma S M, Gupta Y M. 2020. Crystal structure and melting of Fe shock compressed to 273 GPa: In situ x-ray diffraction. Physical Review Letters, 125(21): 215702

Umemoto K, Hirose K, Imada S, Nakajima Y, Komabayashi T, Tsutsui S, Baron A Q R. 2014. Liquid iron-sulfur alloys at outer core conditions by first-principles calculations. Geophysical Research Letters, 41(19): 6712–6717

Umemoto K, Hirose K. 2015. Liquid iron - hydrogen alloys at outer core conditions by first - principles calculations. Geophysical Research Letters, 48(18): 7513–7520

Umemoto K, Hirose K. 2020. Chemical compositions of the outer core examined by first principles calculations. Earth and Planetary Science Letters, 531: 116009

Vočadlo L, Alfè D, Gillan M J, Wood I G, Brodholt J P, Price G D. 2003. Possible thermal and chemical stabilization of body-centred-cubic iron in the Earth's core. Nature, 424(6948): 536–539

Vočadlo L, Dobson D P, Wood I G. 2009. Ab initio calculations of the elasticity of hcp-Fe as a function of temperature at inner-core pressure. Earth and Planetary Science Letters, 288(3–4): 534–538

Wade J, Wood B J. 2005. Core formation and the oxidation state of the Earth. Earth and Planetary Science Letters, 236(1–2): 78–95

Wang T, Song X D. 2018. Support for equatorial anisotropy of Earth's inner-inner core from seismic interferometry at low latitudes. Physics of the Earth and Planetary Interiors, 276: 247–257

Wang W Z, Li Y G, Brodholt J, Vočadlo L, Walter M, Wu Z Q. 2021. Strong shear softening induced by superionic hydrogen in Earth's inner core. Earth and Planetary Science Letters, 568: 117014

Wang W Z, Walter M J, Brodholt J P, Huang S C. 2024. Early planetesimal differentiation and late accretion shaped Earth's nitrogen budget. Nature Communications, 15(1): 4169

Williams Q, Jeanloz R, Bass J, Svendsen B, Ahrens T J. 1987. The melting curve of iron to 250 gigapascals: A constraint on the temperature at Earth′s center. Science, 236(4798): 181–182

Wilson A J, Alfè D, Walker A M, Davies C J. 2023. Can homogeneous nucleation resolve the inner core nucleation paradox? Earth and Planetary Science Letters, 614: 118176

Wilson A J, Pozzo M, Alfè D, Walker A M, Greenwood S, Pommier A, Davies C J. 2022. Powering earth's ancient dynamo with silicon precipitation. Geophysical Research Letters, 49(22): e2022GL100692

Wilson A J, Walker A M, Alfè D, Davies C J. 2021. Probing the nucleation of iron in Earth's core using molecular dynamics simulations of supercooled liquids. Physical Review B, 103(21): 214113

Wood B J, Walter M J, Wade J. 2006. Accretion of the Earth and segregation of its core. Nature, 441: 825–833

Wood B J. 1993. Carbon in the core. Earth and Planetary Science Letters, 117 (3–4): 593–607

Yang H, Dou P X, Xiao T T, Li Y G, Muir J M R, Zhang F W. 2023. The geophysical properties of FeH_x phases under inner core conditions. Geophysical Research Letters, 50(22): e2023GL104493

Yokoo S, Hirose K, Sinmyo R, Tagawa S. 2019. Melting experiments on liquidus phase relations in the Fe-S-O ternary system under core pressures. Geophysical Research Letters, 46(10): 5137–5145

Yoo C S, Holmes N C, Ross M, Webb D J, Pike C. 1993. Shock temperatures and melting of iron at Earth core conditions. Physical Review Letters, 70 (25): 3931

Yoshida S, Sumita I, Kumazawa M. 1996. Growth model of the inner core coupled with the outer core dynamics and the resulting elastic anisotropy. Journal of Geophysical Research: Solid Earth, 101(B12): 28085–28103

Yuan L, Steinle-Neumann G. 2020. Strong sequestration of hydrogen into the Earth's core during planetary differentiation. Geophysical Research Letters, 47(15): e88303

Yuan L, Steinle-Neumann G. 2023. Hydrogen distribution between the Earth's inner and outer core. Earth and Planetary Science Letters, 609: 118084

Zhang B, Ni S, Wu W, Shen Z, Wang W, Sun D, Wu Z. 2023. Small-scale layered structures at the inner core boundary. Nature Communications, 14(1): 6362

Zhang D Z, Jackson J M, Zhao J Y, Sturhahn W, Alp E E, Hu M Y, Toellner T S, Murphy C A, Prakapenka V B. 2016. Temperature of Earth's core constrained from melting of Fe and $Fe_{0.9}Ni_{0.1}$ at high pressures. Earth and Planetary Science Letters, 447: 72–83

Zhang W J, Liu Z Y, Liu Z L, Cai L C. 2015. Melting curves and entropy of melting of iron under Earth's core conditions. Physics of the Earth and Planetary Interiors, 244: 69–77.

Zhang Y J, Luo K, Hou M Q, Driscoll P, Salke N P, Minár J, Prakapenka V B, Greenberg E, Hemley R J, Cohen R E, Lin J F. 2022. Thermal conductivity of Fe-Si alloys and thermal stratification in Earth's core. Proceedings of the National Academy of Sciences of the United States of America, 119(1): e2119001119

Zhang Y J, Wang Y, Huang Y Q, Wang J J, Liang Z X, Hao L, Gao Z P, Li J, Wu Q, Zhang H, Liu Y, Sun J, Lin J F. 2023. Collective motion in hcp-Fe at Earth's inner core conditions. Proceedings of the National Academy of Sciences of the United States of America, 120(41): e2309952120

Zhang Z G, Csányi G, Alfè D, Zhang Y G, Li J, Liu J. 2022. Free energies of Fe-O-Si ternary liquids at high temperatures and pressures: Implications for the evolution of the earth's core composition. Geophysical Research Letters, 49(4): e2021GL096749

（本文责任编辑：龚超颖；英文审校：张兴春）